People's Democratic Republic of Algeria
Ministry of Higher Education and Scientific Research

University M'Hamed BOUGARA – Boumerdes

Institute of Electrical and Electronic Engineering

Department of Electronics

Final Year Project Report Presented in Partial Fulfilment of
the Requirements for the Degree of

MASTER

In **Telecommunication**

Option: **Telecommunications**

Title:

Contribution to The Design and Analysis of a Miniaturized Butterfly MIMO Antenna

Presented by:

- **Rania Yasmine BIR**

Supervisor:

Pr.Arab AZRAR

Registration Number:……/2023

Dedication

For my younger self and my beloved family,

This commitment is a source of deep gratitude to both the courageous spirit within me and my incredible family's unflagging support.

To my younger self,

I am dedicating this work and these words to the version of me that was always willing to follow her dreams, full of curiosity and endless imagination. To the younger me who experienced setbacks and moments of doubt, stumbled and fell, failed and learned how to believe in herself. Through the countless hours of hard work, you have shown me the power of perseverance and the strength that lies within you. Today, as I stand here having completed my master's degree, I am filled with immense pride and gratitude for the journey we have undertaken.

To my beloved family,

I know that I would not be here without your support. I am so grateful for your unconditional love. You have always been there for me, through thick and thin. You have encouraged me to follow my dreams, and you have always believed in me. I am so lucky to have you in my life. I dedicate this work to you. Thank you for everything.

Acknowledgment

I would like to express my heartfelt gratitude to my supervisor, **Pr.Arab AZRAR**, for his invaluable guidance, support, and mentorship throughout the duration of this project. His expertise, patience, and encouragement have been instrumental in shaping the direction and quality of this work. His insightful feedback and constructive criticism have pushed me to expand my horizons and strive for excellence. I am deeply grateful for their dedication and belief in my abilities.

I would like to express my sincere gratitude to **Pr.Abdelhakim DAHIMENE** for his invaluable guidance and assistance throughout this journey. His support has been important in the successful completion of this endeavor.

I am truly fortunate to have had the privilege of working with such remarkable individuals who have invested their time, knowledge, and faith in me. Their contributions have played a significant role in the success of this project, and I am deeply indebted to them.

Lastly, I would like to extend my gratitude to all those who have directly or indirectly contributed to this project but cannot be mentioned individually. Your support, whether in the form of resources, encouragement, or collaboration, has been invaluable, and I am grateful for the collective effort that has made this endeavor possible.

Thank you all for being a part of this journey and for the impact you have had on both my personal and academic growth.

Abstract

In this project, an improved butterfly microstrip antenna is designed, analyzed, and used as elements in a 2×1 Multiple Input Multiple Output MIMO antenna. The antenna design incorporates a butterfly shape derived from a mathematical equation and utilizes a scaling factor to determine the operating frequencies. The initial design is further improved using a super-shape formula and ellipses to approach the real butterfly. The design is done at UHF band around 900 MHz. The research demonstrates that the proposed butterfly microstrip antenna functions effectively as both a microstrip and a monopole antenna. Compared to the original design, the dimensions of the initial antenna are reduced by approximately 54%.

The work is further extended to a 2×1 MIMO antenna using the improved butterfly patches. The MIMO antenna consists of two configurations: one based on the microstrip butterfly patch and the other utilizing the monopole patch. In both structures, the isolation level is lower than -15 dB, and the one based on microstrip resulted in a self-isolated structure with a satisfactory performance.

Contents

List of Figures

List of Tables

List of Abbreviations

d Distance between the patch and the ground of a monopole antenna

d' Distance between the upper adjacent wings in the MIMO antenna

d_{12} Distance from one feed-line to the other one in the MIMO antenna

g Inset gap size

S Scattering parameter

3D Three-Dimensional

BW Band Width

CCL Channel Capacity Loss

dB Decibels (relative to a 1 Watt)

DG Diversity Gain

ECC Envelope Correlation Coefficient

FR-4 Flame Resistant 4

GSM Global System for Mobile communications

HFSS High-Frequency Structure Simulator

HPBW Half Power BeamWidth

L Length

Max Maximum

MEG Mean Effective Gain

MIMO Multiple Input Multiple Output

PCB Printed Circuit Board

RF Radio Frequency

SISO Single Input Single Output

SMA connector Sub-Miniature version A connector

TARC Total Active Reflection Coefficient

UHF Ultra High Frequency

VSWR Voltage Standing Wave Ratio

W Width

General Introduction

Throughout history, the enigmatic allure of radio waves has fascinated thinkers from ancient times to the present day. Radio waves, which are electromagnetic radiation, are capable of transmitting information in space. In enabling wireless communications, antennas are key devices for the transmission of and reception of these waves. As these waves move through the medium and transcend physical boundaries, the human imagination is always captivated by the fascinating magic surrounding them.

In today's world, characterized by widespread and instantaneous wireless communication, the marvel of radio has gone mainstream. Microstrip patch antennas (MPAs) have emerged as a popular choice for a range of applications due to their distinctive qualities, including minimal profile design, lightweight construction, ease of manufacture, affordability, and flexibility. Over the past four decades, MPAs have undergone extensive study and development, contributing significantly to the field of planar antennas. Recent innovations in microstrip antenna designs have led to new shapes and configurations, expanding the possibilities for developing novel and improved antenna types, such as the proposed butterfly-shaped antenna in this project.

An antenna's role extends beyond simple transmission and reception in wireless communication systems. The integration of multiple Input Multiple Output (MIMO) techniques further amplifies the importance of antennas. MIMO uses a number of antennas to increase communication performance by exploiting geographic diversity as well as multipath propagation at the transmitter and receiver end. This technology enables higher data rates, improved signal quality, and increased channel capacity. MIMO technology enables modern wireless systems to achieve remarkable gains in efficiency, reliability, and spectral efficiency.

In this project, our focus is on the design, fabrication, and analysis of improved butterfly-shaped antennas. The report comprises three chapters, beginning with an exploration of antennas and their parameters, along with an overview of microstrip technology and the fundamentals of MIMO techniques. The second chapter delves into a comprehensive literature review on the proposed butterfly geometry, and the modifications that are added to the structure aiming to emulate the intricate shape of a real butterfly. Our improved antenna structure is designed using FR-4 substrate material, and resonates at 900 MHz GSM band as both microstrip and monopole patches. Finally, in chapter three, the improved butterfly antennas are utilized to design 2×1 MIMO systems, leveraging spatial diversity, with an evaluation of their performance. Comparative analysis is conducted against conventional rectangular patches for 2×1 MIMO antennas.

The report ends with a general conclusion where the main results derived from the analysis are summarized and suggestions for future work are presented.

Chapter 1

Generalities

1.1 Introduction

A thorough understanding of antennas and the propagation of electromagnetic waves is necessary in order to take full advantage of radio communications, radar systems, satellites as well as other electronic communication systems. The development of such systems and communications techniques is directly associated with the development of antennas [1]. The fundamentals of antennas, from definition to their basic properties and functions, are covered in this chapter. As microstrip and MIMO antennas are the subject of this project, there will be a focus on them along with the used miniaturization technique.

1.2 Antenna Definition

An antenna is required in the field of communication systems anytime the requirement for wireless communication emerges. An antenna is capable of delivering or receiving electromagnetic waves for the purpose of communication in areas where a wire system cannot be installed [1] [2].

An antenna is a type of transducer that converts electromagnetic fields to alternating current (AC) fields or vice versa. The receiving antenna intercepts electromagnetic energy and provides AC to electronic equipment, whereas the transmitting antenna receives AC from electronic equipment and generates an electromagnetic field. The same antenna can be used for both transmission and reception in two-way communication [2].

1.3 Antenna Types

Antennas have evolved significantly in terms of size and form. They come in a variety of shapes and sizes to suit a wide range of applications. Antennas can be divided into four major types based on their physical construction [1]–[3]. This study provides a quick overview of these types.

- **Wire Antennas** mainly the short dipole and the dipole antennas, the loop antenna, and the monopole antenna.
- **Aperture Antennas** as the slot antennas, horn antennas, and waveguide antennas.

- **Reflector Antennas** as the parabolic reflector and the corner reflector antennas.
- **Microstrip Antennas** microstrip patch antenna, microstrip slot/travelling antenna and printed dipole antenna.

1.4 Antenna Parameters

Definitions of numerous parameters are required to explain the performance of an antenna. Some of the factors are connected, and not all of them must be stated in order to fully describe the antenna's performance. This report covers the critical parameters for characterizing and analyzing an antenna's performance.

1.4.1 Radiation Pattern

A radiation pattern, also known as an antenna pattern, is a graphical representation of an antenna's radiation parameters as a function of spatial coordinates [1]. That is, the design of the antenna determines how the antenna radiates energy into space (or how it receives energy). Radiation properties include power flux density, radiation intensity, field strength, directivity, phase, and polarization. As it radiates in space, the radiation pattern is three-dimensional, and it is frequently expressed utilizing the principle plane patterns which can be formed by cutting two slices across the 3D pattern at the pattern's highest value or by direct measurement. These basic plane designs are commonly known as antenna patterns. The pattern is composed of lobes, a major lobe, and other side lobes, as seen in Figure 1.1. We may deduce the maximum radiation direction and different beamwidths from the plane patterns [1] [2].

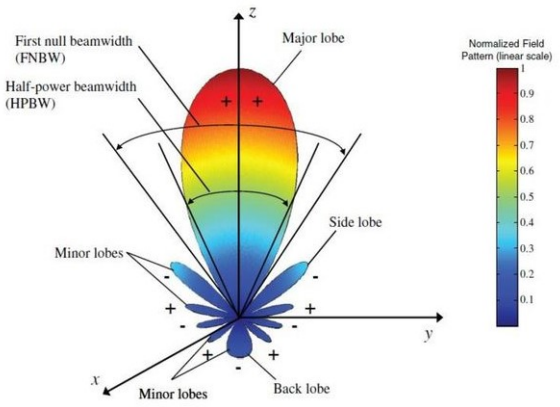

Figure 1.1 Antenna radiation pattern [1].

1.4.2 Directivity and Gain

The directivity is a measure that describes the directional properties of the antenna, it evaluates its capacity to concentrate energy in a certain direction when transmitting or to receive energy better from a specific direction when receiving [1]. The directivity of an antenna is defined mathematically (Equation 1.1) as the ratio of the intensity of radiation in a particular direction from the antenna to the average intensity of radiation in all directions [2]. The average radiation intensity is equal to the total power emitted by the antenna divided by 4π.

$$D(\theta,\phi) = 4\pi \frac{U(\theta,\phi)}{P_{rad}} \tag{1.1}$$

Where, $D(\theta,\phi)$ is the directivity, $U(\theta,\phi)$ is the radiation intensity, and P_{rad} is the total radiated power.

An antenna can be omnidirectional if it receives signals equally from all directions, or directional if it draws in signals better from one direction. It can detect a weaker or more distant signal than an equivalent omnidirectional antenna in this direction [2].

The gain is the ability of the antenna to increase the power to be emitted. It is defined as the ratio of power transmitted in a certain direction with a specific reference point [2].

The gain of the antenna, denoted $G(\theta,\phi)$, is related to the directivity by the amount of the power radiated by the antenna from the input power which is called the radiation efficiency η [2].

$$G(\theta,\phi) = \frac{P_{rad}}{P_{in}} D(\theta,\phi) = \eta D(\theta,\phi) \tag{1.2}$$

1.4.3 Beamwidths

The angular separation between two identical locations on opposing sides of the main lobe is defined as the beamwidth of a pattern. There are several beamwidths in an antenna pattern. The Half Power Beamwidth (HPBW) is one of the most often used beamwidths, and it is defined as the angle between two directions on a plane encompassing the direction of the maximum of a beam in which the radiation intensity is half of the beam's maximum value. It is also known as the 3dB beamwidth. Another critical beamwidth is the angular spacing between the pattern's initial nulls, which is known as the First-Null Beamwidth (FNBW). Both beamwidths, are illustrated in Figure 1.1 [1] [2].

1.4.4 Polarization

The polarization of the wave produced by the antenna (antenna polarization) is the property of an electromagnetic wave that describes the time-varying direction and relative amplitude of the electric-field vector at a fixed point in space. Depending on the antenna shape and excitation mechanism, the polarization can be linear, circular, or elliptical [2]. These types are illustrated in Figure 1.2.

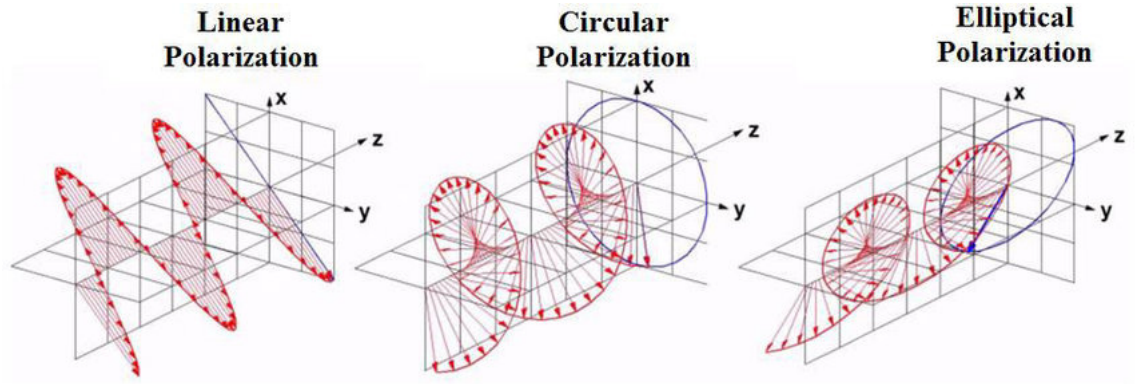

Figure 1.2 Polarization types: linear, circular, and elliptical polarization [4].

- **Linear polarization** at a given location in space, a time-harmonic wave is linearly polarized if the electric-field (or magnetic-field) vector is constantly orientated along the same straight line at every moment of time.

- **Circular polarization** if the electric (or magnetic) field vector at a particular location in space follows a circle as a function of time, the wave is circularly polarized.
- **Elliptical polarization** if the point of the field vector (electric or magnetic) tracks an elliptical locus in space, the time-harmonic wave is elliptically polarized. At various points in time, the field vector varies continuously with time, describing an elliptical locus.

There are also the terms co-polarization and cross-polarization are frequently used to describe the polarization purity of the linearly polarized antennas. Co-polar indicates the electric field component parallel to the polarization line, whereas, the cross-polar is the component perpendicular to it.

The co-polarized, E_{co}, and cross-polarized, E_{cross}, components of an antenna polarized along the Oy axis are defined by Ludwing [5] as

$$\begin{bmatrix} E_{co} \\ E_{cross} \end{bmatrix} = \begin{bmatrix} sin\phi & cos\phi \\ cos\phi & -sin\phi \end{bmatrix} \begin{bmatrix} E_\theta \\ E_\phi \end{bmatrix} \tag{1.3}$$

If the antenna is polarized along the Ox axis, then, the E_{co} and E_{cross} are expressed as

$$\begin{bmatrix} E_{co} \\ E_{cross} \end{bmatrix} = \begin{bmatrix} cos\phi & -sin\phi \\ sin\phi & cos\phi \end{bmatrix} \begin{bmatrix} E_\theta \\ E_\phi \end{bmatrix} \tag{1.4}$$

An antenna has a good polarization purity if the cross component is $-20dB$ lower than the co-polar component [2]. This level may increase in some antenna systems as the MIMO system.

1.4.5 Reflection Coefficient

The reflection coefficient describes the quantity of electromagnetic energy reflected as a result of an impedance mismatch in the transmission medium. It is a measure of the antenna's ability to convey power from a source, and is hence related to impedance matching [2].

The voltage reflection coefficient, denoted Γ (or S_{11} as S-paramater), is defined as the ratio of the reflected voltage amplitude to the incident voltage amplitude [2].

The return loss, denoted RL, is typically used in combination with the reflection coefficient and is simply defined as the ratio of the incident power of the antenna to the power reflected back from the antenna. It is expressed mathematically as

$$RL(dB) = 10Log_{10}(\frac{P_{in}}{P_{ref}}) \tag{1.5}$$

It may also be represented in terms of the magnitude of the reflection coefficient as

$$RL(dB) = -20Log_{10}(|\Gamma|) \tag{1.6}$$

1.4.6 Antenna Bandwidth and Resonant Frequency

The bandwidth is a range of frequencies across which the antenna can function successfully. Many antennas operate in a resonant mode, which allows them to deliver high performance over a relatively small bandwidth [2].

The bandwidth is defined as the frequency range where the magnitude of input reflection coefficient is less than -10 dB and the antenna is matched to the feed line under the same condition. The

resonant frequency, which may be used as the operating frequency, is the frequency at which the input reflection coefficient is the smallest. Typically, an antenna is constructed by first determining its size in proportion to a desired resonance frequency. The plot of the magnitude of the input reflection coefficient versus frequency is commonly used to determine the antenna's bandwidth and resonant frequency [2].

1.5 Microstrip Antennas

1.5.1 History

Deschanp designed microstrip antennas in 1953, based on the unwanted radiation impact of microstrip lines. Previously, it was more typical to avoid rather than investigate the occurrence. Lewin was the first to examine radiation emitted by microstrip discontinuities. They received little attention until the early 1970s, when a new need developed for compact, lightweight antennas in a range of applications. Vigorous research operations have recently taken place, prompted in part by the efforts of the Air Rome Development Center, Hanscom AFB, Massachusetts, and the development of this family of antennas has finally progressed into a new era with products that are significantly different from their predecessor [6].

1.5.2 Definition and Basic Characteristics

A microstrip or patch antenna is a metal patch installed at ground level with a dielectric substance of a certain thickness in between. These are small antennas with little radiation. A microstrip antenna is made out of a very thin metallic strip placed on a ground plane and sandwiched by a dielectric substance. the metallic patch is comprised of thin copper foil that has been plated with a corrosion-resistant metal such as gold, tin, or nickel. The patch is the component in charge of power radiation. For simplicity of analysis and manufacture, the patch or microstrip is typically square, circular, or rectangular in form. The picture below depicts a micro-strip or patch antenna. In this regard, the current initiative contributes to the investigation of butterfly-shaped patch formations [7].

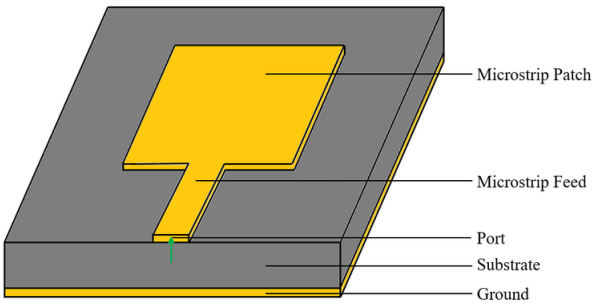

Figure 1.3 Microstrip antenna configuration [7].

There are several substrates that may be utilized to create microstrip antennas, with relative dielectric constants typically in the range 2.2 to 12. The proper selection of dielectric material and thickness is critical when developing a microstrip patch antenna [1].

1.5.3 Feeding Techniques

There are several configurations available for feeding microstrip antennas. Microstrip lines, coaxial probes, aperture coupling, and proximity coupling are the four most common.

Microstrip line feed is one of the simplest techniques to construct since it is simply a conducting strip connected to the patch and can thus be considered an extension of the patch. It is easy to model and match by adjusting the inset position. The problem with this method is that as substrate thickness grows, so does surface wave and spurious feed radiation, limiting the bandwidth [8].

1.5.4 Fringing Effect

As we feed the patch, electromagnetic waves begin to couple between the patch and the ground. In most areas of the patch, antenna radiation flows directly from the patch to the ground; however, near the patch's borders, antenna radiation moves in the air before reaching the ground. This percentage of the electromagnetic waves that went through the air is known as the fringing of electromagnetic waves, and this phenomena is known as the fringing effect [9]. Figure 1.4 illustrates the fringing fields in a microstrip patch antenna.

The performance of a microstrip antenna is greatly influenced by fringing fields. In microstrip antennas, the electric filed at the patch's center is zero. The radiation is caused by the fringing field that exists between the patch's edge and the ground plane.

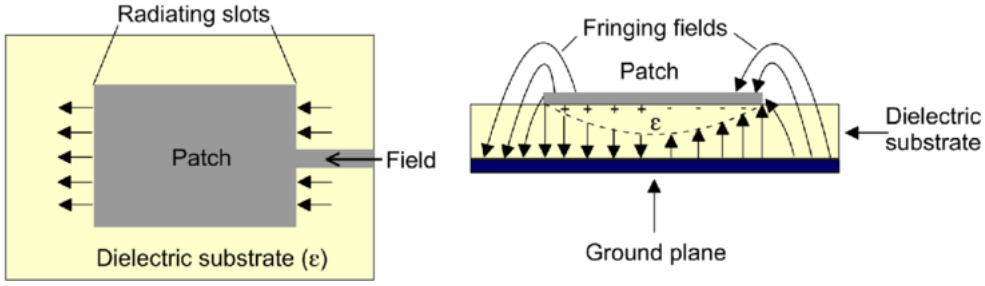

Figure 1.4 Top and side views of a microstrip antenna and the fringing fields [10].

1.6 Miniaturization Technique: Defected Microstrip Structure

A Defected Microstrip Structure (DMS) is created by etching some uniform or non-uniform slits or patterns over a microstrip structure which modifies its electromagnetic properties. The defect's shape, size, and location are carefully designed to control the propagation, impedance, and radiation properties of the microstrip structure [11].

Introducing a defect changes the antenna's effective electrical length resulting in a shift in its resonant frequency. The design and optimization of DMS structures require careful consideration of the geometry and placement of the defects to achieve specific desired properties [11].

Defects in the patch's high current distribution regions result in a longer electrical length, which lowers the resonant frequency. It is an efficient method for reducing the size of the antenna without affecting its radiation properties [11].

1.7 MIMO Concept

Designing very high-speed wireless links with good quality of service and range capability in the environments where the line of sight is not applicable is a significant research and engineering challenge. One of the most emerging techniques for this purpose is the Multiple-Input-Multiple-Output, also known as MIMO [12].

MIMO technique is a cutting-edge technology that uses multiple transmit and receive antennas to achieve multipath propagation and meet the higher data rate and the quality demands of modern wireless communications. MIMO communication distributes the data as numerous signals across several antennas at the same time, all while using a single radio channel. At the transmission point, the data is divided into various data streams and recombined on the receiving end by another MIMO system with the same number of antennas. The receiver is built to accommodate for the minor time delay between signal receptions, any added noise or interference, and even lost transmissions [13].

MIMO was first proposed as a feasible solution for overcoming the data rate limitations of Single-Input- Single-Output (SISO) systems in the early 1990s. Furthermore, MIMO can be used in various networks to improve channel capacity, system reliability, and data transmission speed by utilizing the highest capacity of wireless communication systems. The great improvement in the wireless communication performance made this technology expected to play a fundamental role in the advance of the future mobile generations as the 5G and beyond [13]. Figure 1.5 represents a block diagram of a 4×4 MIMO system. As it is illustrated, there are 4 antennas at the transmitting side and another 4 at the receiving side. Each receiver can receive signals from all the transmitters.

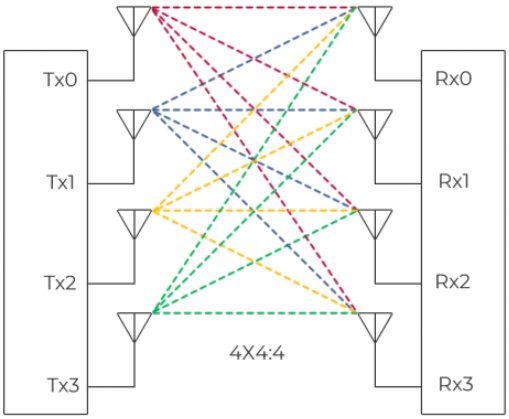

Figure 1.5 Block diagram of a 4×4 MIMO system [14].

MIMO radios enable redundancy in data transmission that traditional single antenna configurations (SISO: Single Input Single Output) cannot provide by delivering the same data on several streams. As a result, MIMO systems have significant benefits over traditional SISO configurations [12] [13]:

- Higher data rates: MIMO allows several data streams to be delivered concurrently by employing multiple antennas at both sides of the communication link, increasing the overall data rate.
- Increased reliability: MIMO overcomes the effects of fading and interference, which can result in errors in the communication network, by employing numerous antennas.

- Higher capacity: the capacity of the system increases as the number of antennas in the transmitting and the receiving sides increase.
- Efficient spectrum utilization: increased data capacity without requiring additional bandwidth.

1.8 Diversity

Array antennas have become essential components in mobile communications, serving not only as base station antennas but also integrated within mobile handsets. Their purpose within handsets is to enable antenna diversity, a technique that employs multiple antennas to enhance the quality of wireless connections. This technique leverages the combination or selection of antennas to maximize signal strength during reception, particularly in environments with multiple signal paths caused by reflections and obstacles [15] [16].

In urban and indoor settings, direct line-of-sight between the base station and the mobile handset is often unavailable. Instead, the transmitted signal undergoes numerous reflections along various paths before reaching the receiver. Each reflection introduces a potential phase shift, and when combined with time delays, these multiple signal paths can interfere destructively at the receiver's antenna location, resulting in significant signal fade and potential loss of the transmission link [15] [16].

By utilizing two or more receiving antennas, each antenna experiences a distinct interference environment. If these receiving antennas are spatially separated, differently oriented, or possess different reception patterns, it is highly likely that at least one of the antennas, or a subset thereof, will encounter a signal of sufficient strength to maintain a reliable connection. The antenna diversity can take the following forms [15] [16].

1.8.1 Space Diversity

Space diversity, also known as antenna diversity, refers to the utilization of multiple antennas at either the transmitter or receiver end (or both). By physically separating the antennas in space, the aim is to overcome the issue of fading. However, when it comes to microstrip MIMO antennas, the antennas are designed to be in close proximity to achieve a compact structure. In such scenarios, a significant challenge arises in the form of mutual coupling reduction [15].

1.8.2 Polarization Diversity

Polarization diversity involves sending and receiving signals using several antennas with different polarization. Pairs of linearly polarized antennas should be orthogonal placed to achieve polarization diversity. This technique can significantly decrease the mutual coupling within the system. Polarization and space diversities can be combined for further improvement of the MIMO antenna performance [15].

1.8.3 Radiation pattern Diversity

It refers to the utilization of antennas with different directivities which help in selecting several multipath components [15].

1.9 Mutual Coupling

In an antenna array, the distance between the adjacent patches is of great importance due to the influence of one antenna element on the performance of the others. This phenomenon is called mutual coupling and it is the result of the close proximity and interaction between antennas in a system [1].

In MIMO systems, each antenna should operate independently of the others. The mutual coupling in MIMO systems decreases the isolation between the antennas which results in interference and correlation, which reduce the benefit from the multiple signal paths. The mutual coupling also affects the radiation properties of the system resulting in lower system performance. These problems caused by the mutual coupling in MIMO systems reduce the freedom in simultaneous and independent data streaming [17].

Increasing the distance between the antennas is not always a good solution for mutual coupling since compact size is desired in microstrip technology. There exist different techniques intended for decoupling. Introducing isolation structures, adding parasitic elements, or using decoupling networks, can be employed to reduce mutual coupling between antennas. Algorithms can be employed to compensate for the problem, for instance, the MIMO channel calibration at the level of signal processing, and adaptive beamforming [17].

1.10 Quality Measures

The evaluation of the MIMO system performance is based on certain measures. The system can be further optimized according to the levels of these parameters [18]. The significance of these measures are presented as follows:

1.10.1 Mutual Coupling

Mutual coupling is defined as the energy absorbed by an antenna by its adjacent radiating antenna. The radiation pattern, reflection coefficient, and input impedance of MIMO antennas are influenced by mutual coupling. The mutual coupling depends on the configuration of the array as well as its interaction with other elements. It is represented as, usually in dB, the *S*-parameter of the *ith* antenna on the *jth* antenna [1].

1.10.2 Envelope Correlation Coefficient

Envelope Correlation Coefficient, or ECC, quantifies the correlation between the amplitudes (or envelopes) of the signals received at different antennas. The ECC value has to be 0; however, its true value shall not exceed 0.5. The calculation of the envelope correlation coefficient, for two ports system, is carried out by the following equation [19]

$$ECC = \frac{|S_{11}^{*}S_{12} + S_{21}^{*}S_{22}|^2}{(1-|S_{11}|^2-|S_{21}|^2)(1-|S_{22}|^2-|S_{12}|^2)} \tag{1.7}$$

1.10.3 Diversity Gain

The improvement of system reliability and performance which can be achieved with the use of a series of antennas is referred to as diversity gain. The diversity gain, denoted DG, quantifies

the strength of a MIMO system to counter fading and signal degradation caused by multipath propagation. MIMO systems can become more reliable, thereby reducing impact of fadings, through the use of spatial diversity. The DG is dependent on ECC and it is defined as [19]

$$DG = 10\sqrt{1 - ECC^2} \tag{1.8}$$

It should equal to 10 as the signals are not correlated.

1.10.4 Total Active Reflection Coefficient

Total Active Reflection Coefficient, or the TARC, characterizes the overall reflection performance of the MIMO system. It is defined as the ratio of the incident power to the squared value of the reflected power. For a two-port system, the TARC is expressed as [19]

$$TARC = \sqrt{\frac{|S_{11} + S_{12}e^{j\theta}|^2 + |S_{21} + S_{22}e^{j\theta}|^2}{2}} \tag{1.9}$$

where θ is the excitation signal's phase. It is arbitrary, and the environment helps in further randomizing this phase [19].

1.10.5 Mean Effective Gain

The Mean Effective Gain, denoted MEG, describes the ability of the antenna to receive the signal. The best value for the MEG is -3 dB. It is described by the following formula [20].

$$MEG_i = 0.5\left[1 - \sum_{j=1}^{N} |S_{ij}|^2\right], i = 1,2 \tag{1.10}$$

where N is the number of antenna elements.

1.10.6 Channel Capacity Loss

The Channel Capacity Loss, or CCL, is the term used to describe the maximum message rate that can be transmitted through a communication channel without encountering any loss, and it should be less than 0.4 bits/s/Hz in general. It is expressed as [19]

$$CCL = -\log_2\left(det\begin{bmatrix} 1 - |S_{11}|^2 - |S_{12}|^2 & -(S_{11}^* S_{12} + S_{21}^* S_{22}) \\ -(S_{22}^* S_{21} + S_{12}^* S_{11}) & 1 - |S_{22}|^2 - |S_{21}|^2 \end{bmatrix}\right) \tag{1.11}$$

1.11 Design of Microstrip Patch Antennas

Figure 1.6 depicts the design procedures for a microstrip antenna. The most important stage is to complete the design requirements which are determined by the application. Typically, antenna parameters are provided by the system engineer following a system-level study and simulation of the entire system. System requirements determine antenna characteristics such as operating frequency, bandwidth, gain, radiation pattern, and polarization. The first step in developing a printed antenna is to select a suitable substrate. Following the collection of design requirements, the following stage is to pick the radiating element, antenna size, feeding mechanism, and electromagnetic modeling approach required to get antenna performance [21].

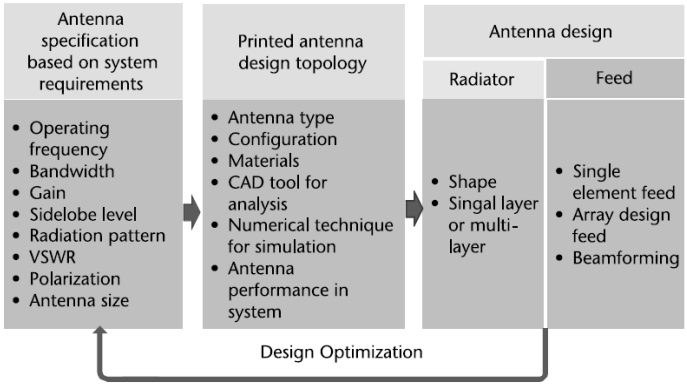

Figure 1.6 Microstrip patch antenna design flow [21].

Figure 1.7 illustrates a flowchart outlining the sequential steps involved in the design of a microstrip antenna with a single element. The design process commences by establishing the antenna specifications tailored to the specific application requirements. The selection of substrate material is then determined based on both the specifications and cost considerations. Empirical equations are employed to ascertain the radiating properties of the antenna and to determine the appropriate feed design parameters. Electromagnetic simulation-based Electronic Design Automation (EDA) technologies are utilized to optimize the antenna's performance. Once the design parameters have been fine-tuned, a printed circuit board (PCB) for the antenna is prepared for manufacturing. Finally, comprehensive measurements are conducted to evaluate all the antenna's characteristics prior to its utilization, as referenced in [21].

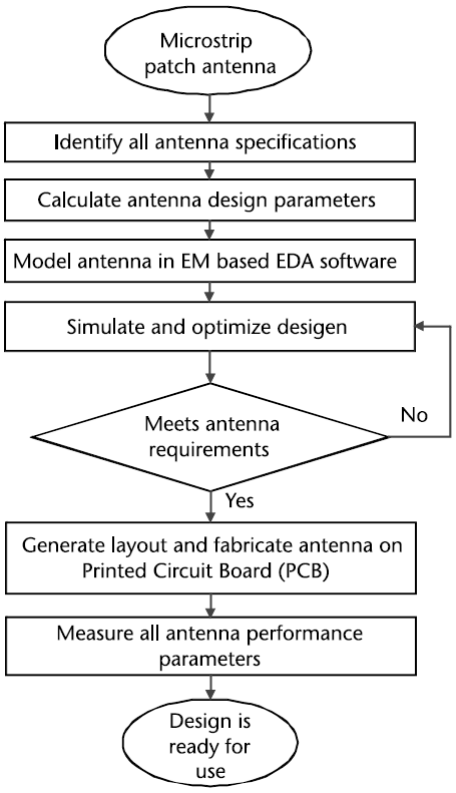

Figure 1.7 Microstrip antenna design and fabrication process [21].

1.11.1 Benefits and Drawbacks

The adaptability of microstrip antennas is their most prominent advantage. For starters, they are compact and lightweight, and they conform well to planar and non-planar surfaces. Furthermore, when placed on hard surfaces, they can be mechanically robust. Another advantage of microstrip antennas is their ease of fabrication and low cost. These low-profile antennas are suitable for direct printing onto a circuit board [1] [22].

one downside of microstrip antennas is their low efficiency. Furthermore, they have low power, poor polarization purity, poor scan performance, and incorrect feed radiation. Moreover, these antennas have a very limited frequency bandwidth, which may be advantageous for some government security systems [1] [22].

While certain defects may be corrected, doing so might have a detrimental impact on the antenna's effectiveness in other ways. Increasing the height of the substrate, for example, can increase the efficiency of the antenna. As the antenna's height grows, more surface waves will pass through the substrate, scattering at bends and surface imperfections and decreasing the pattern and polarization [1].

1.11.2 Applications

T Microstrip patch antennas offer numerous advantages that outweigh their disadvantages, including ease of construction and their lightweight nature. These attributes contribute to their wide range of applications. Microstrip patch antennas find applications in diverse fields such as medicine, satellite communications, and military systems like rockets, aircraft, and missiles. Their popularity extends across industries and regions due to their commercial viability, thanks to the cost-effectiveness of substrate materials and production processes [9].

1.12 Conclusion

In conclusion, this chapter has provided a comprehensive overview of essential concepts in antenna design and analysis, microstrip technology,and MIMO technique. This overview will serve as a foundation for the forthcoming chapters.

Chapter 2

Improved Butterfly Patch Design

2.1 Introduction

A PCB, or Printed Circuit Board, antenna is an antenna that is directly incorporated onto a PCB. It is a cost-effective and efficient method of incorporating an antenna into a product design, especially when space is restricted [21].

PCB antennas are created using microstrip antenna concepts. They are typically constructed by etching a conductive pattern on one or both sides of a PCB substrate, which serves as the antenna's radiating element. The radiating element's properties, such as length, width, and shape, are carefully chosen to get the desired resonance frequency and radiation pattern [1] [21]. Patch antennas come in a variety of forms and sizes, the most popular of which being rectangular and circular patch antennas [1]. Nevertheless, any continuous form may be explored, and a number of designs, such as a butterfly-shaped patch antenna, are proposed and studied. Based on prior work [9], a contribution to the shape of the proposed butterfly patch is made in this study, with the goal of approaching the natural shape of a butterfly. The butterfly shape is motivated by the fact that the structure embedded in MIMO system presents low mutual coupling as demonstrated in chapter 3.

2.2 Butterfly Geometry Description

2.2.1 Butterfly Construction

As was proposed in the previous work, the butterfly form is obtained by combining sine and cosine functions with specified values. The equation is given as [9]

$$\begin{cases} x = R\cos(\theta) \\ y = R\sin(\theta) \end{cases} \quad 0 \leq \theta \leq 2\pi \tag{2.1}$$

where,

$$R = m(R_1 + R_2) \tag{2.2}$$

$$R_1 = 9 - 0.5\sin(\theta) + 2.5\sin(3\theta) + 2\sin(5\theta) - 1.7\sin(7\theta) \tag{2.3}$$

$$R_2 = 3cos(2\theta) - 2cos(4\theta) - 0.4cos(16\theta) \tag{2.4}$$

The parameter m in Equation 2.2 is a real positive number which fixes the dimensions of the patch [9]. Figure 2.1 shows the output of drawing the set of equation 2.1.

Figure 2.1 Proposed butterfly shape.

2.2.2 Butterfly Patch Design

The antenna consists of the FR-4-epoxy dielectric substrate of thickness $h = 1.56$ mm, relative permittivity $\varepsilon_r = 4.4$, and loss tangent of $tan(\delta) = 0.02$.

According to the previous research, matching at the fundamental mode frequency could not be achieved even after using the stub and quarter-wave transformer techniques. As a solution, the patch was slightly altered, but without changing the overall shape of the butterfly, by adding a rectangle to the bottom of the structure [9] as shown in Figure 2.2.

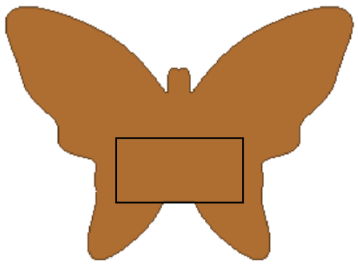

Figure 2.2 Modified Butterfly microstrip antenna.

An inset feed is used with a 50Ω characteristic impedance. The width of the inset feed line is calculated using the following formula [23].

$$W_f = \frac{2h}{\pi}\left[B - 1 - \ln(2B-1) + \frac{\varepsilon_r - 1}{2\varepsilon_r}\left(\ln(B-1) + 0.39 - \frac{0.61}{\varepsilon_r}\right)\right] \tag{2.5}$$

Where,

$$B = \frac{377\pi}{2Z_0\sqrt{\varepsilon_r}} \tag{2.6}$$

This gives $W_f = 2.985$ mm. The inset gap, denoted g, was arbitrarily set to 0.5 mm; a parametric study on the inset gap size will be conducted later in this chapter.

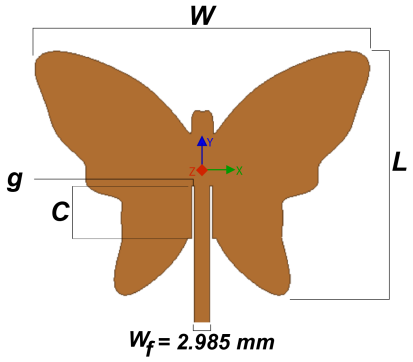

Figure 2.3 Modified butterfly microstrip antenna with inset feed-line.

The dimensions of the butterfly shaped patch are fixed and controlled by the parameter *m*. A parametric study on *m* has been included in the previous research work [9], but since the thickness of the substrate and the simulation software is changed, another parametric study using HFSS software is presented in this work. The results are summarized in Table 2.1.

m	0.5	0.75	1.00	1.25	1.50	1.75	2.00	2.25	2.50	2.75	3.00	3.25	3.50	3.75	4.00	4.25
f(GHz)	7.6	5.2	3.89	3.09	2.55	2.19	1.89	1.68	1.51	1.37	1.26	1.09	1.02	0.99	0.95	0.88

Table 2.1 Butterfly patch antenna first resonant frequency as function of the parameter *m*.

The above results are plotted in the graph depicted in Figure 2.4. This graph facilitates the design of a butterfly patch antenna made of FR-4-epoxy dielectric material. As expected, the resonant frequency decreases as *m* increases. The limitations of *m* are due to the available means for implementing reasonable sizes; however, they can be extended to values other than those shown in the graph, thus the work is open to any other frequencies and dielectric materials.

As depicted in Figure 2.3, both the width, *W*, and the length of the patch, *L*, are fixed by determining the appropriate value for the parameter *m* depending on the desired resonant frequency. The inset distance, *C*, is set to meet the best matching between the patch antenna and the 50 Ω feed line.

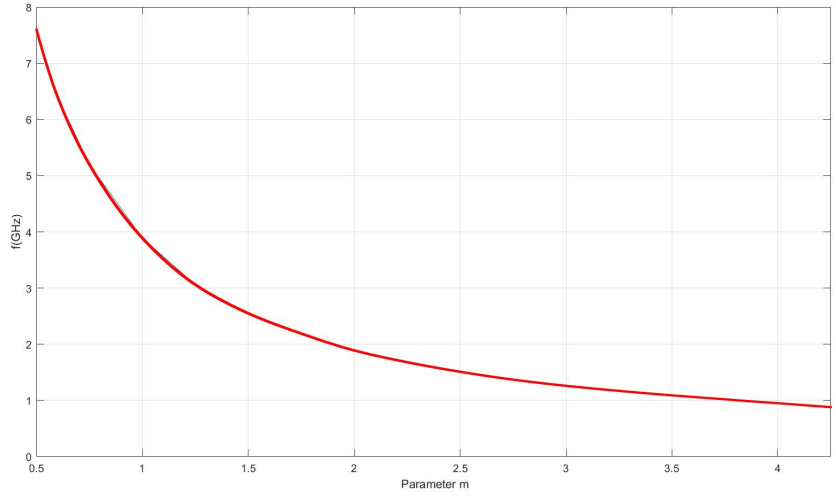

Figure 2.4 First resonant frequency versus the parameter *m*.

2.3 Proposed Design

The proposed structure in this section is intended to approximate the natural shape and patterns found on a real butterfly. Figure 2.5 depicts a variety of butterfly insects from which the newly proposed patch antenna structure was inspired.

Figure 2.5 Butterfly insects [24] [25] [26].

As shown above, the wings are divided into four parts and the patterns that exist on them are almost oval and elliptical. To approach these patterns, the Defected Microstrip Structure, or DMS, was used.

2.3.1 Design Details

Starting from the previously proposed structure depicted in Figure 2.3, different slot shapes are placed on the wings of the butterfly patch aiming to lengthen the electrical length, and thus miniaturizing the patch. The goal is to decrease the resonant frequency of the patch to 900 MHz GSM band. The initial patch is operating at $f_r = 1.66$ GHz (Radio Astronomy 1.66 - 1.6605 GHz [27]), by setting the parameter m to 2.3. The antenna is y-polarized and its dimensions are $W = 63$ mm and $L = 45.8$ mm. Figure 2.6 represents the surface current distribution of the structure of Figure 2.3 where $C = 14$ mm. The figure clearly shows that the length of the edges of the wings represents the main parameter that fixes the resonant frequency because the two nulls of the current exist at the upper and the lower extremities of the wings, whereas the maximum is in the middle. Usually, to lower the resonant frequency, it is necessary to disrupt the maximum current by introducing defects. Remarkably, the position of the maximum current conveniently aligns with a region that facilitates the approximation of the natural butterfly wings shape by introducing special defects. These defects effectively divide each wing into two sub-wings, enhancing the resemblance to actual butterfly wings.

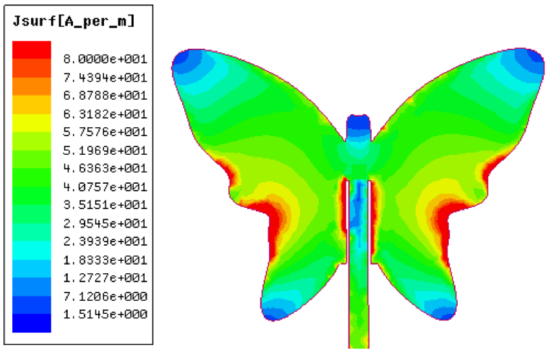

Figure 2.6 Surface current distribution of the basic structure of the patch antenna.

The first modification is to introduce special defect, as said before, based on the super-shape formula given by [28]

$$\begin{cases} x = R\cos(\theta) \\ y = R\sin(\theta) \end{cases} \quad 0 \leq \theta \leq 2\pi \tag{2.7}$$

Where,

$$R = \left[\left| \frac{1}{a}\cos\left(n_0 \frac{\theta}{4}\right) \right|^{n_1} + \left| \frac{1}{b}\sin\left(n_0 \frac{\theta}{4}\right) \right|^{n_2} \right]^{-1/n_3} \tag{2.8}$$

where a, b, n_0, n_1, n_2, and n_3 real numbers.

The required 2D shape is obtained by setting the equation parameters to $a = 7$, $b = 5$, $n_0 = 2$, $n_1 = 0.3$, $n_2 = 1$, and $n_3 = 0.3$, which gives the shape illustrated in Figure 2.7.

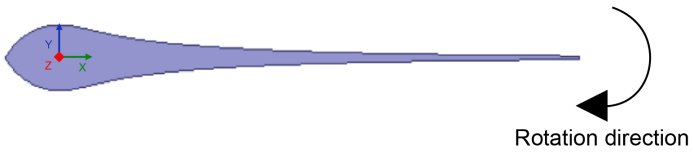

Figure 2.7 Super-shape.

The super-shape was scaled by 0.2, rotated by 190°, and moved by a vector of coordinates (-17.1, -7.3, 0); then mirrored and duplicated with respect to the center of the coordinates system (see Figure 2.3 for the center of the coordinates system position). The super-shapes are then subtracted from the original butterfly structure as illustrated in Figure 2.8.

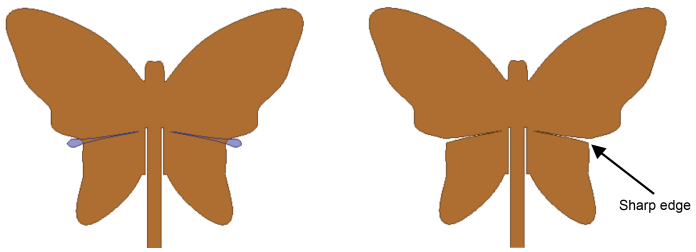

(a) Before **(b)** After

Figure 2.8 Butterfly patch structure with four wings.

For rounded wing edges, other polyline shapes are subtracted from the structure. The polyline constituts of 6 points that are connected using the three point arc tool in HFSS software. The points are (-15.23 ,-10.86 ,1.56), (-14 ,-8 ,1.56), (-11.04 ,-6.38 ,1.56), (-13.5 ,-6.5 ,1.56), (-15.5 ,-7.5 ,1.56), and (-15.23 ,-10.86 ,1.56). The shape is then duplicated and mirrored with respect to

the center of the coordinates system and subtracted from the structure. Figure 2.9 illustrates the resultant structure.

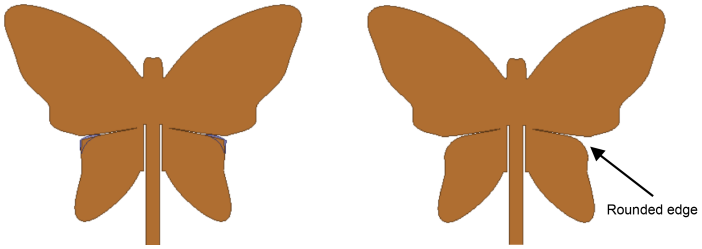

(a) Before **(b)** After

Figure 2.9 Butterfly structure before and after the first modification.

By incorporating these slots into the antenna design, the initial current distribution is effectively redistributed. This redistribution leads to a concentration of the maximum current around the newly introduced super-shape, thereby creating a longer path for the current to flow. As a consequence, this alteration in the current path has resulted in a notable decrease in the resonant frequency, which now stands at $f_r = 1.343$ GHz.

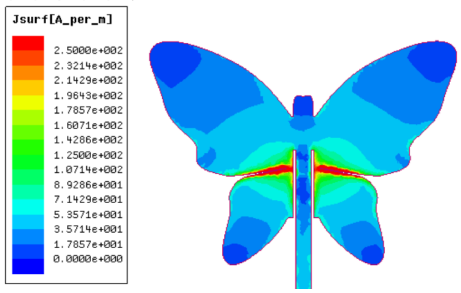

Figure 2.10 Surface current distribution after the first modification.

To further decrease the resonant frequency and achieve a closer resemblance to the natural butterfly wings, additional defects are introduced. These defects are strategically placed in areas where the surface current exists. Specifically, the same defect is replicated with a scaling factor of 0.32, rotated by 155°, and shifted by a vector of coordinates (-18.5, 3, 0). Furthermore, an ellipse with a center at (-21.2, 1.5, 1.63), a major axis of 3.55 mm, a ratio of 0.325, and a rotation of $-45°$ is incorporated. These shapes are duplicated and mirrored relative to the center of the coordinate system. Finally, they are subtracted from the butterfly patch, as depicted in Figure 2.11.

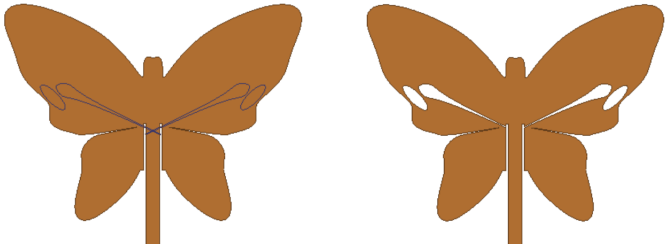

(a) Before **(b)** After

Figure 2.11 Butterfly structure before and after the second modification.

The introduced modifications results in a surface current distribution that is depicted in Figure 2.12, where the electrical length is further lengthened leading to a resonant frequency of $f_r = 0.896$ GHz.

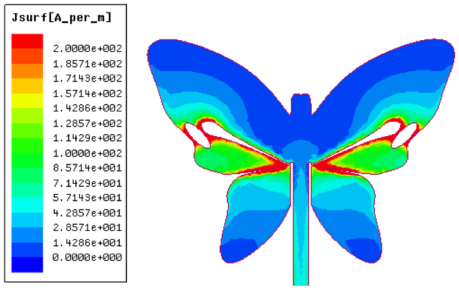

Figure 2.12 Surface current distribution after the second modification.

The distribution of surface current is almost negligible at the top and bottom edges of the wings. Consequently, adding slots in these surfaces will not have a significant effect on the resonant frequency. To take advantage of this remark, further ellipses have been added to the edges of the structure. The addition of these defects is motivated by the willingness of approaching the natural patterns of butterfly wings. All the added ellipses have 0.325 ratio; the details are summarized in Table 2.2.

Center Point	Major Axis (*mm*)	Rotated by (°)
(-6.5, -17.9, 1.56)	1	55
(-8.6, -20.3, 1.56)	1	50
(-11.1, -22.3, 1.56)	1	40
(-14, -23.4, 1.56)	1	10
(-27.7, 10.8, 1.56)	1	-60
(-26.8, 8.1, 1.56)	1	-60
(-25.3, 5.7, 1.56)	1	-60
(-26.3, 14.9, 1.56)	1	-60
(-25.4, 16.5, 1.56)	1	-30
(-15.6, -4.8, 1.56)	1	-10
(-12.8, -5, 1.56)	1	0
(-9.1, 11.5, 1.56)	1	-40
(-11.6, 13, 1.56)	1	-30
(-14.8, -20.5, 1.56)	2	80
(-19.2, -3.5, 1.56)	2	-30
(-15.2, 15, 1.56)	2	-30
(-19.9, 17.2, 1.56)	2	-20
(-28.8, 17.5, 1.56)	2	150
(-28, 14, 1.56)	2	120
(-25.6, 18.8, 1.56)	3	-10

Table 2.2 Ellipses dimensions.

The introduction of these ellipses on the last version of the butterfly patch results in a new structure demonstrated in Figure 2.13.

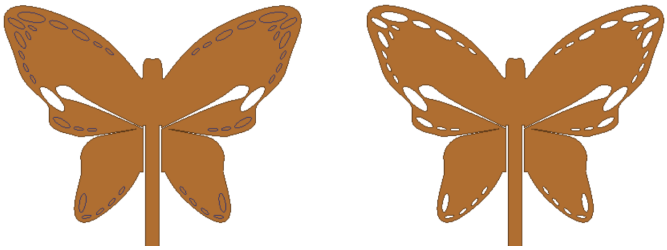

(a) Before **(b)** After

Figure 2.13 Butterfly structure before and after the third modification.

Remark The simulation of the structure showed that the added ellipses have almost no effect on the antenna performance.

The structure shown above can be developed further to mimic the natural pattern found on a butterfly wing. Additional slots have been incorporated using the ellipses listed in Table 2.3.

Ellipse	Center Point	Major Axis (*mm*)	Ratio	Rotated by (°)
1	(-6.7, 3.3, 1.56)	3.55	0.325	-40
2	(-6.7, 3.3, 1.56)	2.5	0.325	-40
3	(-3.9, 12.3, 1.56)	3.75	0.325	-40
4	(-3.5, 12.3, 1.56)	4.0	0.325	-40

Table 2.3 Additional ellipses dimensions.

By subtracting ellipse 2 from ellipse 1, an oval ring slot is created. This resulting shape is then subtracted from the butterfly patch,. Moreover, ellipse 3 has been extracted from ellipse 4 and joined to the antenna patch. These modifications contribute to the final structure, which is depicted in Figure 2.14.

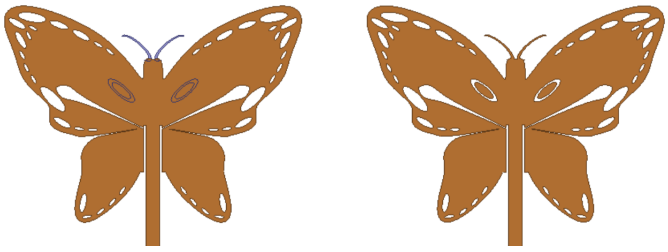

(a) Before **(b)** After

Figure 2.14 Butterfly structure before and after the final modification.

The surface current distribution of the final structure is shown in Figure 2.15. As expected, it is similar to the previous surface current distribution depicted in Figure 2.12 since the added ellipses are placed in the non-radiating edges of the patch.

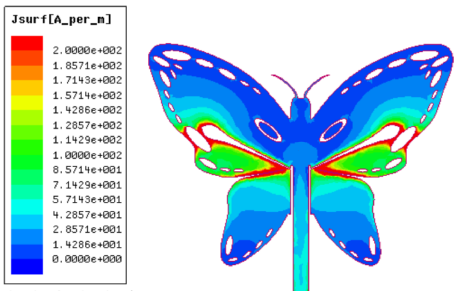

Figure 2.15 Surface current distribution of the final butterfly patch structure.

Figure 2.16 represents the evolution of the butterfly shaped antenna. Labeled by (a)-(e), each depicts the previously discussed steps. To see the effect of each modification, the magnitude of the input reflection coefficient is illustrated in Figure 2.17.

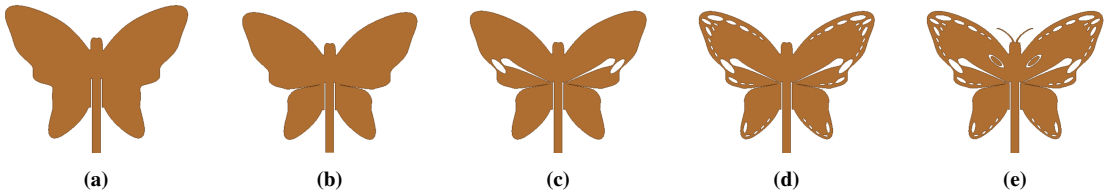

Figure 2.16 Evolution of the microstrip butterfly patch antenna design.

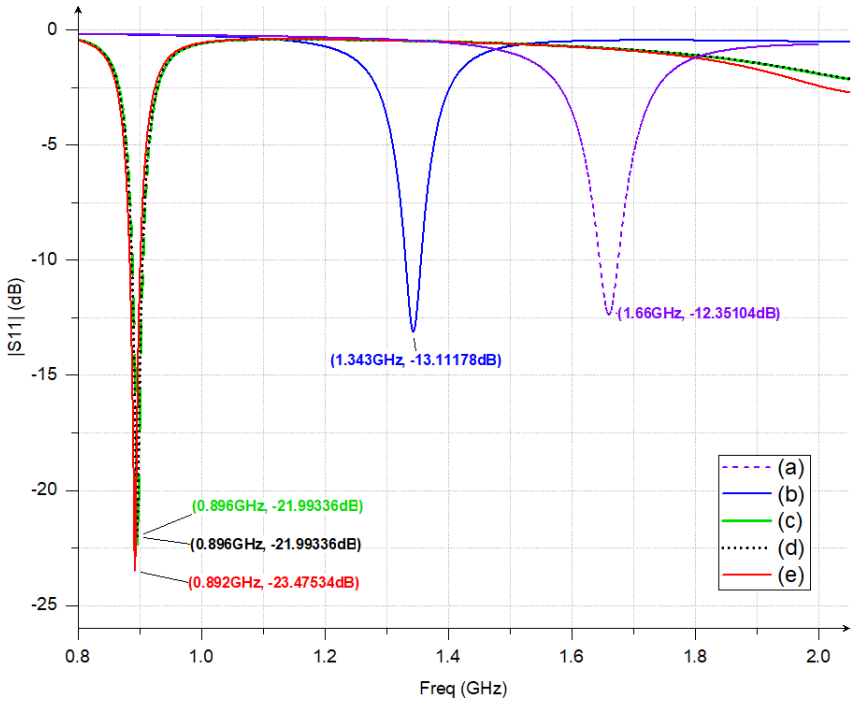

Figure 2.17 Input reflection coefficient evolution of the microstrip butterfly patch antenna.

A parametric study on the inset feed-line gap has been performed in order to achieve the exact desired frequency of 900 MHz. Figure 2.18 depicts the input reflection coefficient for several

inset gap size g. In addition to the already arbitrarily chosen gap size $g = 0.5$ mm, the gap size is reduced from $g = \frac{W_f}{4}$ to $g = \frac{W_f}{15}$. The decrease in the the gap width leads to a decrease in the resonant frequency and an increase the corresponding level of the input reflection coefficient. Consequently, the best value that results in both the desired frequency with the best match is $g = \frac{W_f}{4}$.

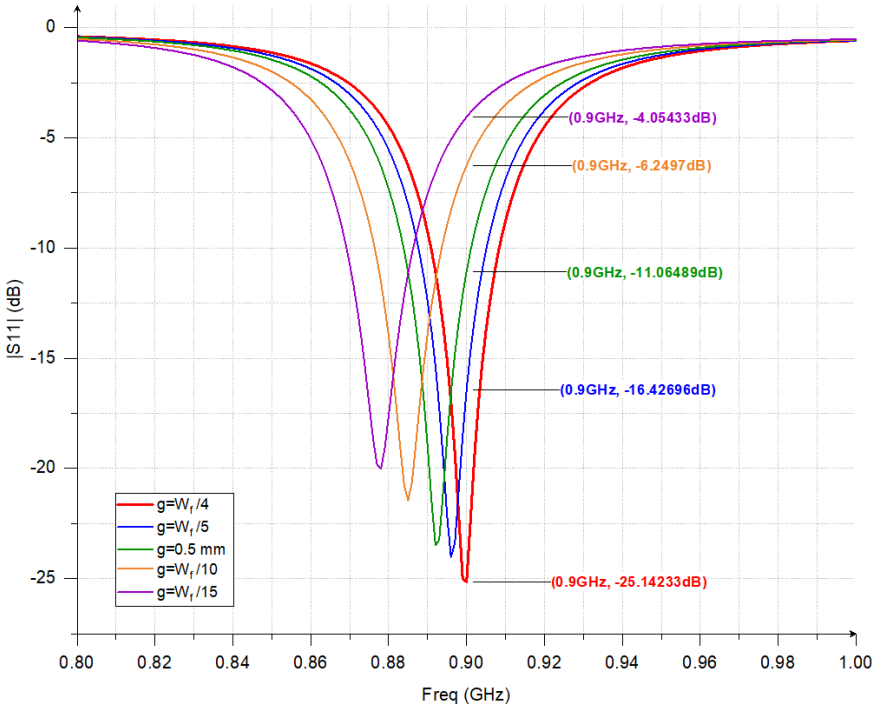

Figure 2.18 First resonant frequency of the final butterfly structure for different values of the inset gap g.

2.3.2 Results and discussion

The final proposed design of the improved microstrip butterfly patch is illustrated in Figure 2.19. The input reflection coefficient of this microstrip butterfly antenna with an 80mm×60mm ground plane beneath the structure is illustrated in Figure 2.20.

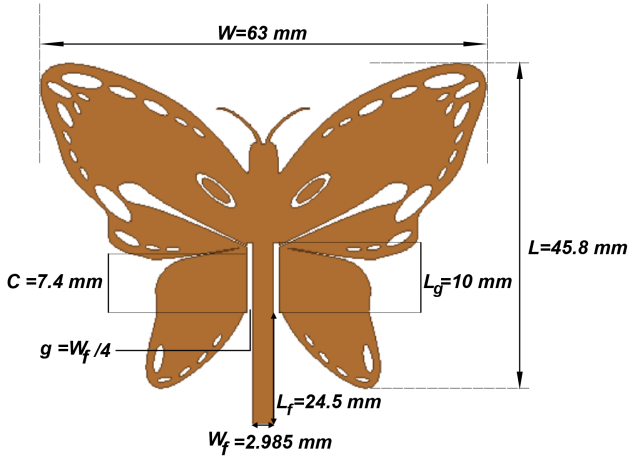

Figure 2.19 Geometry of the final design of the improved microstrip butterfly patch.

As illustrated in Figure 2.20, the butterfly patch antenna is resonating at 900 MHz. The -10 dB Bandwidth is calculated using the following formula [2].

$$BW\% = \frac{f_2 - f_1}{f_1 + f_2} \times 200 \tag{2.9}$$

where f_1 is the lower frequency and f_2 is the higher frequency of the operating bandwidth, leading to 2% bandwidth. This value indicates that the structure is a narrow band antenna. This value will be improved in the monopole antenna case.

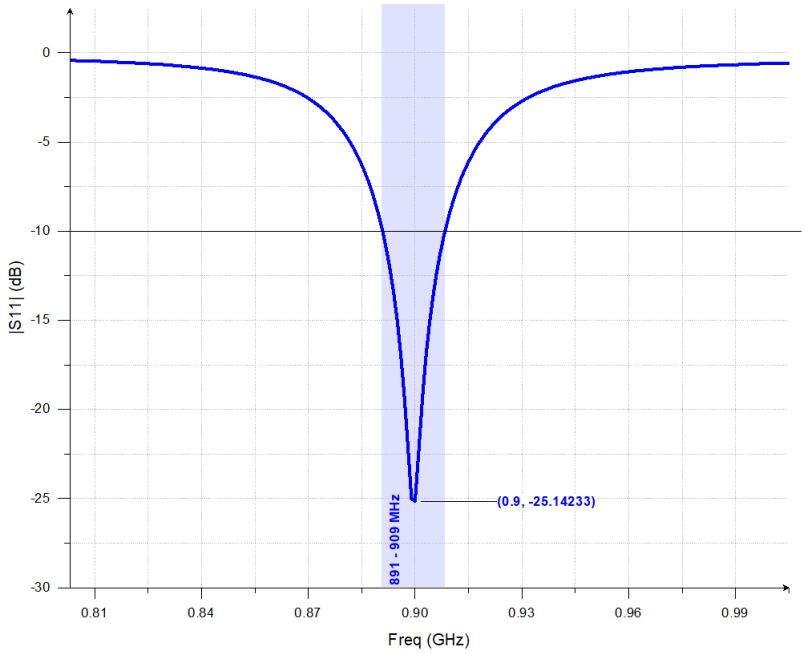

Figure 2.20 Input reflection coefficient of the final design of the proposed microstrip butterfly patch.

As compared to the initial butterfly structure, and at 900 MHz, the improved structure is reduced in size. Figure 2.21 represents the butterfly patch resonating at 900 MHz before and after the modifications. Quantitatively, the width was reduced from 115 mm to 63 mm, and the length from 85 mm to 45.8 mm, amounts to approximately a 54% reduction.

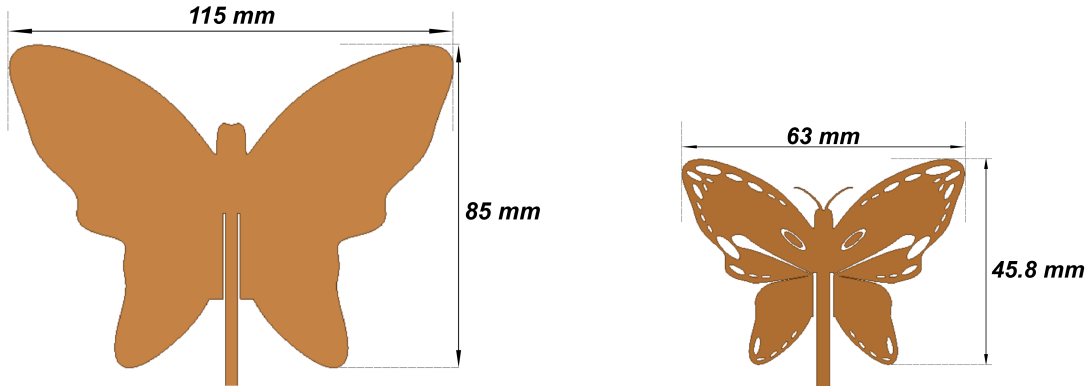

(a) Before **(b)** After

Figure 2.21 Butterfly patch antenna structure before and after modifications operating at 900 MHz.

As already illustrated in Figure 2.15, The surface current distribution is concentrated at the radiating edges of the patch around the cut made in the middle of the wings.

To have a global view of the radiation properties of the structure, the 3D radiation pattern at 900 MHz is illustrated in Figure 2.22. The components of the field add in phase in the direction perpendicular to the ground plane yielding a maximum radiation normal to the patch. It contains only one main lobe in the z-direction. The figure clearly shows that the butterfly microstrip antenna is a directional broadside radiating antenna.

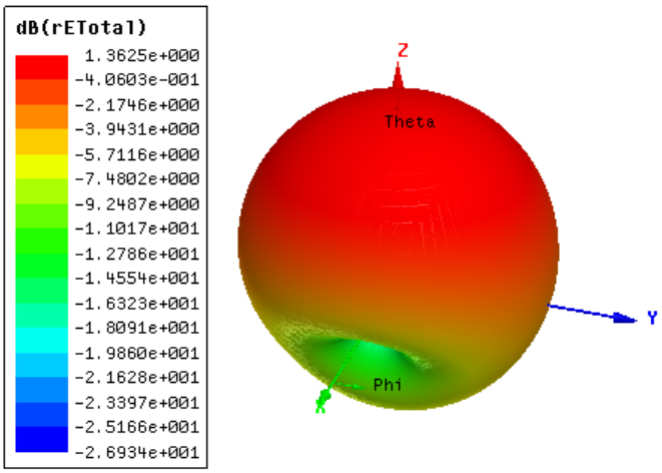

Figure 2.22 3D polar radiation pattern of the final proposed microstrip butterfly patch in dB.

To have a better description of the electromagnetic radiation, the principle plane patterns are represented in Figure 2.23. It is apparent that there is some back radiation and it is due to the finite ground plane. Equation 1.3 lists the co-polar and the cross-polar components of the y-polarized antenna. The level of the cross-polar components shown in Figure 2.24 is lower than -40 dB for the E-field and -20 dB for the H-field. More details are presented in Table 2.4.

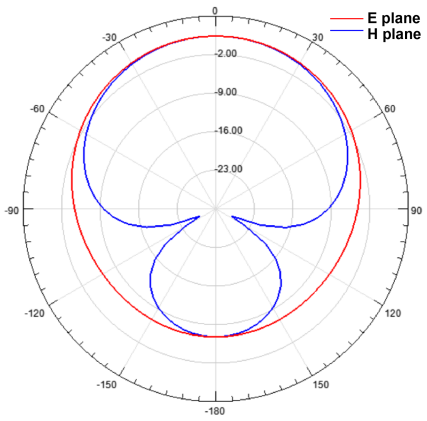

Figure 2.23 E and H plane patterns of the final proposed microstrip butterfly patch in dB.

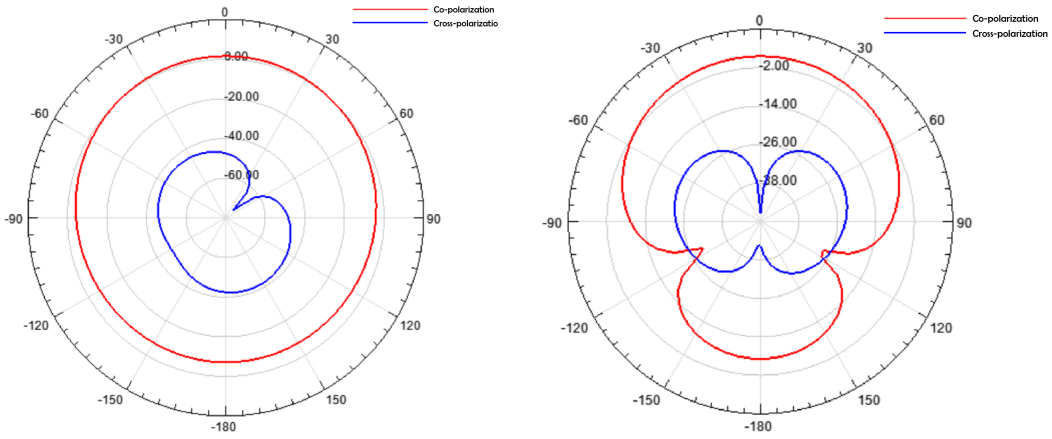

(a) E ($\phi = 90°$). **(b)** H ($\phi = 0°$).

Figure 2.24 Co-polar and cross-polar components of the improved microstrip butterfly patch.

Plane	Max co-polar component	Max cross-polar component	HPBW	Max Directivity	Max Gain
E($\phi = 90°$)	1.36 dB at $\theta = 0°$	-41.32 dB at $\theta = 60°$	122°	-3.61 dB at $\theta = 0°$	-16.41 dB at $\theta = 0°$
H($\phi = 0°$)	1.36 dB at $\theta = 0°$	-21.86 dB at $\theta = -60°$	102°	-3.61 dB at $\theta = 0°$	-16.41 dB at $\theta = 0°$

Table 2.4 Improved microstrip butterfly antenna at 900 MHz.

2.4 Monopole Butterfly Patch antenna

A microstrip monopole patch antenna consists of a microstrip fed patch on top of a partially grounded dielectric [29]. In this section, the same structure of the butterfly antenna depicted in Figure 2.19 is used as monopole antenna. The ground exists only under the feed line as shown in the coming figures. The distance between the ground and the patch is of great importance [29].

2.4.1 Microstrip feed monopole antenna

In the monopole case, the inset feeding technique is not required, the microstrip feed line is used, and the size of the line is kept unchanged for 50 Ω characteristic impedance. Figure 2.25 shows the structure of the proposed monopole antenna. The ground size is set to 13.4 mm × 72 mm and a parametric study on the distance between the patch and the ground, denoted d, is conducted.

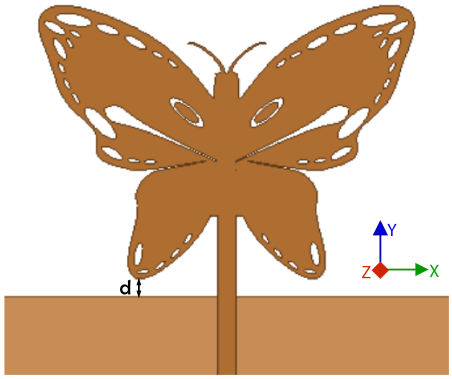

Figure 2.25 Butterfly monopole patch antenna with a microstrip feed-line.

Figure 2.26 represents the input reflection coefficient for different values of d. Three values for d were simulated and the best in terms of matching and bandwidth was chosen, $d = 1.0$ mm. This choice resulted in a bandwidth of about 101.83 % around 1.084 GHz.

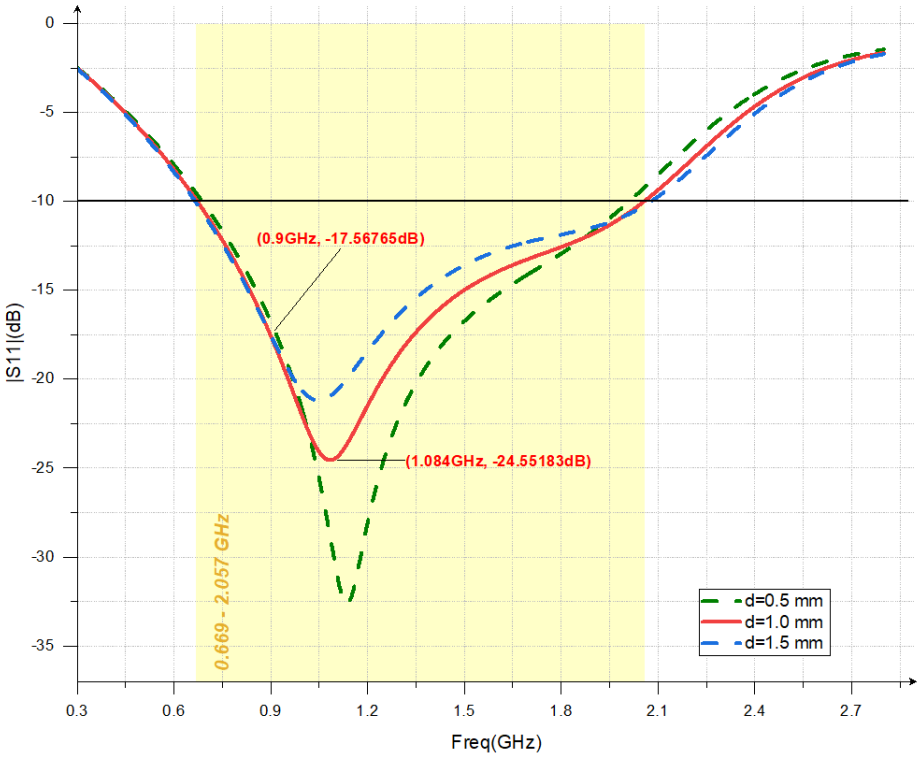

Figure 2.26 Input reflection coefficient of the proposed monopole butterfly patch for different values of d.

2.4.1.1 Surface Current Distribution

Figure 2.27 displays the surface current distribution of the proposed antenna structure at two distinct frequencies: 900 MHz and 1.8 GHz within the bandwidth. At both frequencies, a null current exists at the upper and lower wings of the antenna, while the main concentration of the surface current is observed along the feed-line, as well as in the middle region of the wings, with a notable variation between the two operating frequencies. At 900 MHz, the current distribution along the feed-line is more pronounced, indicating a better matching at this frequency. Consequently, the current intensity on the feed-line is higher at 900 MHz compared to 1.8 GHz.

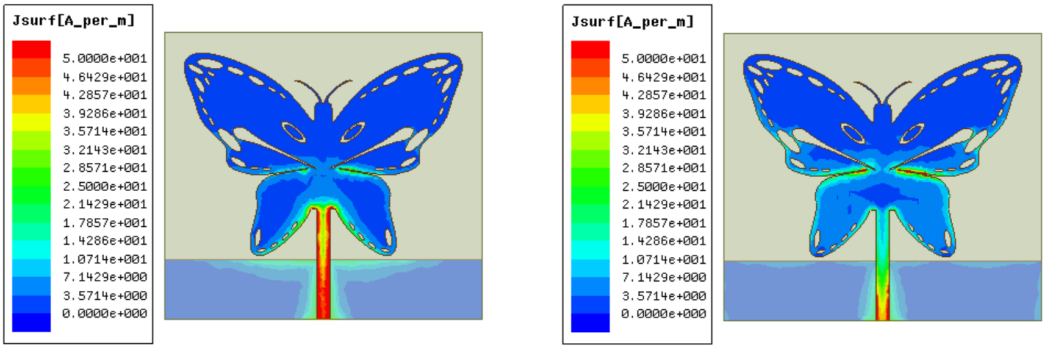

(a) at 900 MHz. **(b)** at 1.8 GHz.

Figure 2.27 Surface current distribution of the proposed monopole butterfly antenna at 900 MHz and 1.8 GHz.

2.4.1.2 Radiation Patterns

Unlike the microstrip butterfly case studied previously, the radiated field of the monopole exists in the upper and the lower hemispheres and it is omnidirectional as indicated in Figure 2.28. To better describe the performance of the monopole antenna, the 2D radiation patterns were plotted and depicted in Figure 2.29. In this figure, it is clearly seen that the radiation pattern is similar to a linear half-wave dipole antenna where an 8-shaped form is observed in the E-plane and a circle in the H-plane.

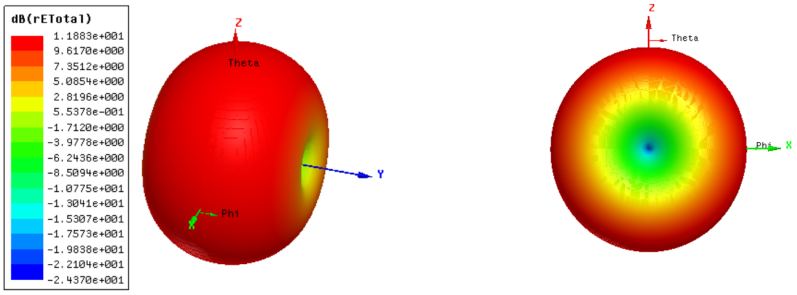

Figure 2.28 3D radiation pattern of the monopole butterfly antenna in dB at 900 MHz.

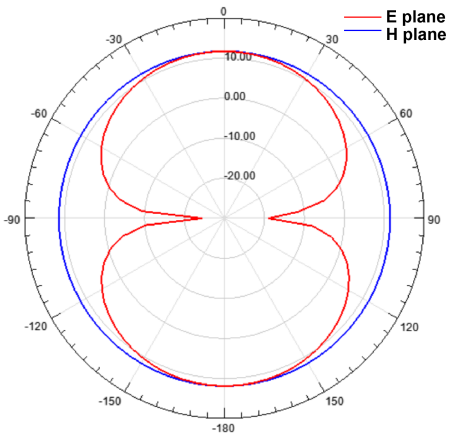

Figure 2.29 E and H plane patterns of the monopole butterfly antenna in dB at 900 MHz.

To see the purity of polarization of the radiated fields of the monopole antenna, the cross-polar components in both planes are compared to the co-polar components as illustrated by Figure

2.30. A -42 dB and -20 dB cross polar levels are observed in the E and H planes respectively. Similarly, the details are summarized in Table 2.5.

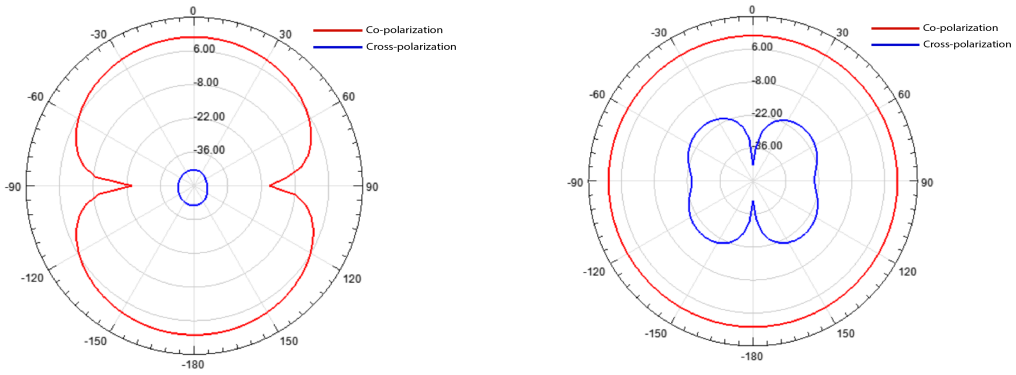

(a) E ($\phi = 90°$). **(b)** H ($\phi = 0°$).

Figure 2.30 Co- and Cross- polar components in dB of the proposed monopole butterfly antenna at 900 MHz.

Plane	Max co-polar component	Max cross-polar component	HPBW	Max Directivity	Max Gain
E($\phi = 90°$)	11.88 dB at $\theta = -180°$	-40.41 dB at $\theta = 165°$	86°	-5.75 dB at $\theta = 0°$	-5.86 dB at $\theta = 0°$
H($\phi = 0°$)	11.88 dB at $\theta = -180°$	-19.73 dB at $\theta = -50°$	Circle	-5.75 dB at $\theta = 0°$	-5.86 dB at $\theta = 0°$

Table 2.5 Butterfly monopole antenna at 900 MHz.

2.4.2 Inset feed monopole antenna

The effect of the inset feed on the monopole antenna is studied in this section. The structure of Figure 2.25 is now fed with an inset feed-line as demonstrated by Figure 2.31 with the same physical dimensions used in the microstrip case (see Figure 2.19).

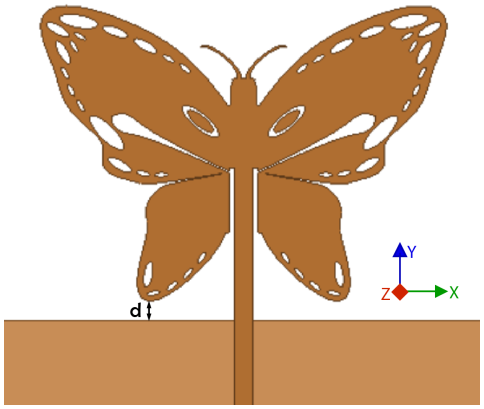

Figure 2.31 Monopole patch antenna with inset feed-line.

The simulation results of the modified monopole patch antenna structure (with a ground size of 13.4 mm × 72 mm) exhibited dual-band characteristics, as depicted in Figure 2.32. Additionally,

a parametric study is conducted to investigate the influence of the distance between the ground and the patch, denoted as d. Among the distances studied, a value of $d = 0.25$ mm is chosen as it demonstrates good matching and bandwidth for both frequency bands.

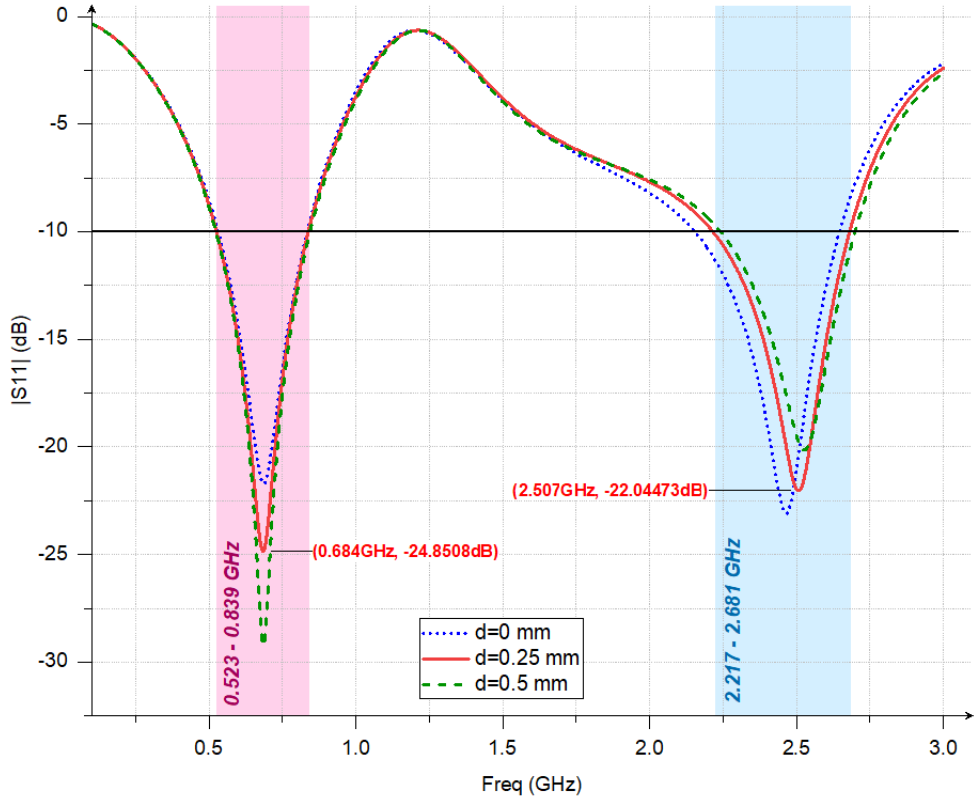

Figure 2.32 Input reflection coefficient of the monopole butterfly antenna with inset feed-line for different values of d.

The achieved bandwidth around 684 MHz amounts to approximately 46.4%, while the bandwidth around 2.507 GHz is approximately 18.95%. Notably, the desired frequency of 900 MHz is not obtained with this specific design. To address this desire, further adjustments to the patch dimensions are required in order to incorporate the 900 MHz frequency within the antenna's operating bandwidth. To recover the 900 MHz, the patch is scaled by a factor of 0.79, with the widths of the feed-line and the inset gap kept unchanged. The resulted input reflection coefficient for different values of the distance between the ground and the patch, d, is depicted in Figure 2.33.

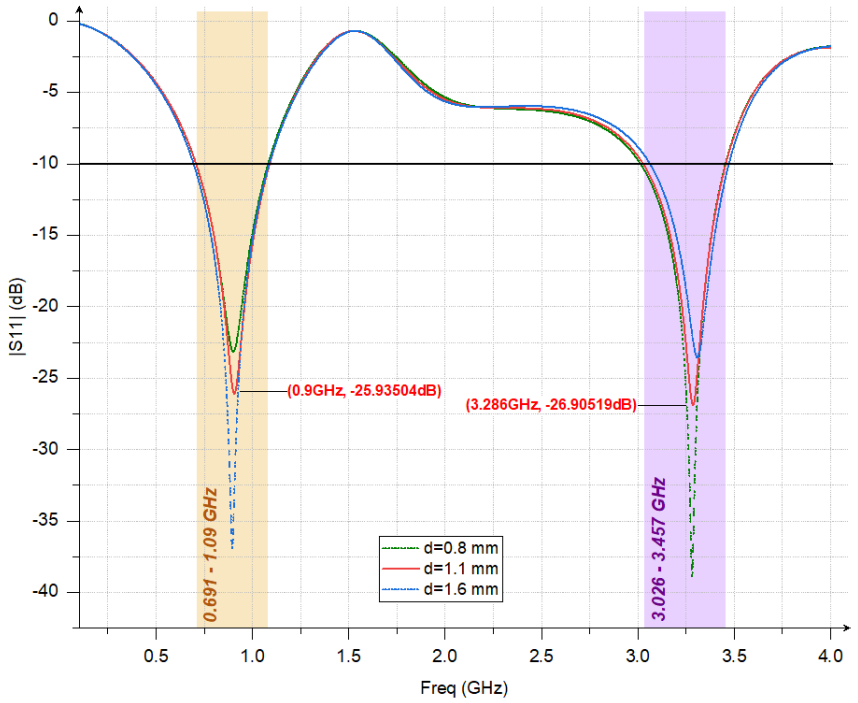

Figure 2.33 Input reflection coefficient of the scaled monopole butterfly antenna with inset feed-line for different values of d.

The value $d = 1.1$ mm is chosen to maintain good matching at both resonant frequencies. With this adjustment, the monopole patch antenna achieved a bandwidth of approximately 44.81% around 900 MHz for the first band, and a bandwidth of approximately 13.30% around the resonant frequency of 3.286 GHz for the second band.

2.4.2.1 Surface Current Distribution

To examine the performance of the antenna, the surface current distribution at the two bands is illustrated in Figure 2.34. The current distributions at the two frequencies are quite similar, the only difference is in the paths which indicate the resonant lengths responsible on the two bands. This leads to similar forms of the fields at the two frequencies.

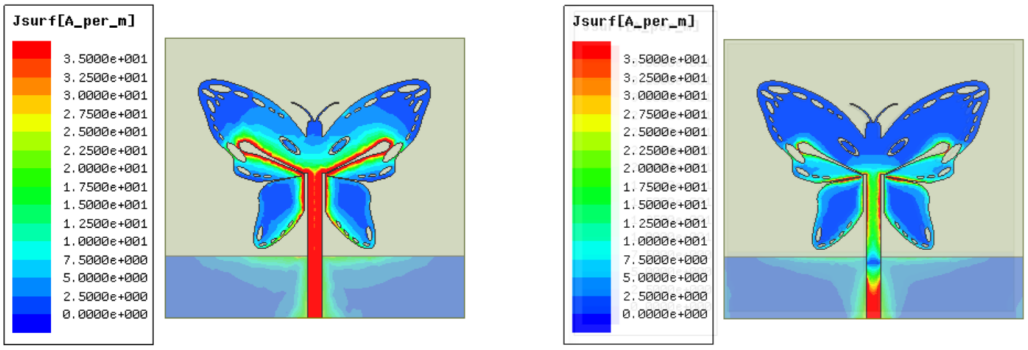

(a) at 900 MHz. **(b)** at 3.286 GHz.

Figure 2.34 Surface current distribution of the scaled monopole butterfly antenna at 900 MHz and 3.286 GHz.

2.4.2.2 Radiation Patterns

As expected, the 3D polar radiation patterns at the two frequencies have similar forms as illustrated in Figure 2.35. The radiation patterns resemble a donut shape, which is typical for dipole antennas. Further insights into the radiation patterns can be gained by examining the 2D patterns of the E and H fields, which are presented in Figure 2.36.

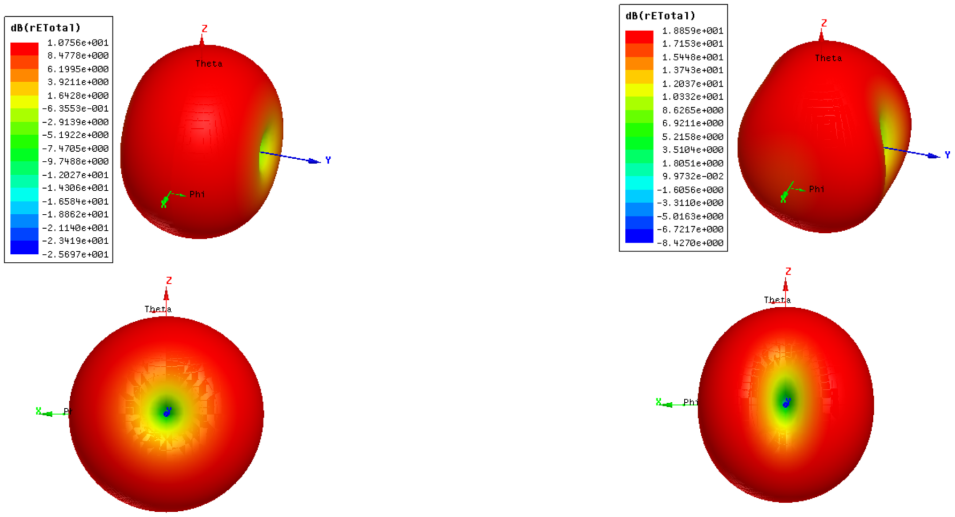

(a) at 900 MHz. **(b)** at 3.286 GHz.

Figure 2.35 3D polar radiation patterns of the scaled monopole butterfly antenna as seen from different views at 900 MHz and 3.286 GHz.

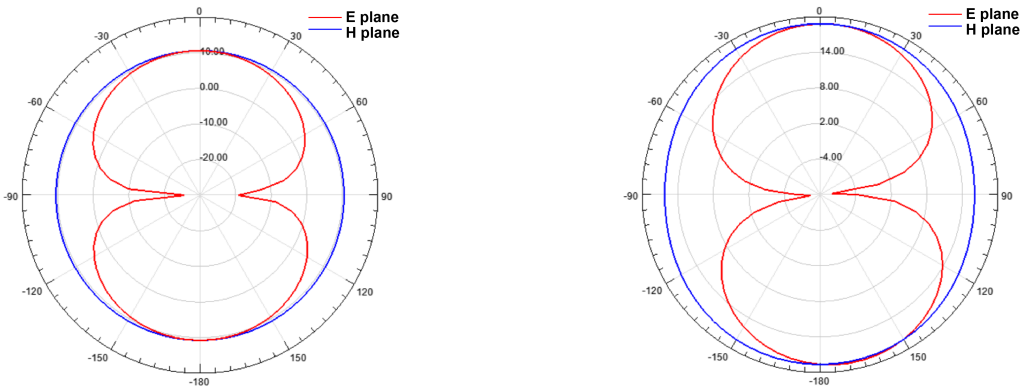

(a) at 900 MHz. **(b)** at 3.286 GHz.

Figure 2.36 E and H plane patterns of the scaled butterfly antenna at 900 MHz and 3.286 GHz.

The polarization purity is studied in Figure 2.37. In the E-plane, the wave is observed to be purely linearly polarized, as the cross-polarization components are negligible. However, in the H-plane, the cross-polarization components are relatively high in directions other than the maximum radiation directions. This can be attributed to the presence of current on the wings of the butterfly patch in diagonal directions. The details are presented in Table 2.6.

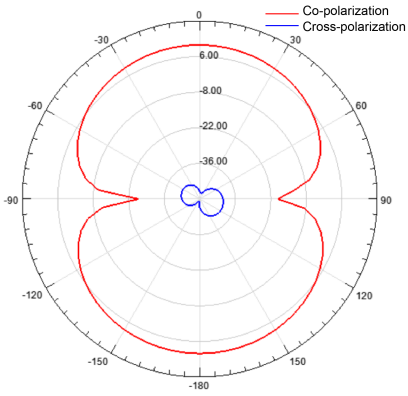

(a) E-plane polar components at 900 MHz.

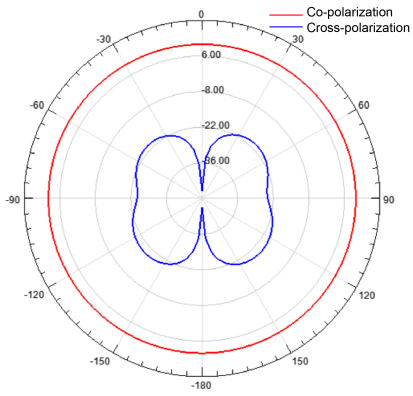

(b) H-plane polar components at 900 MHz.

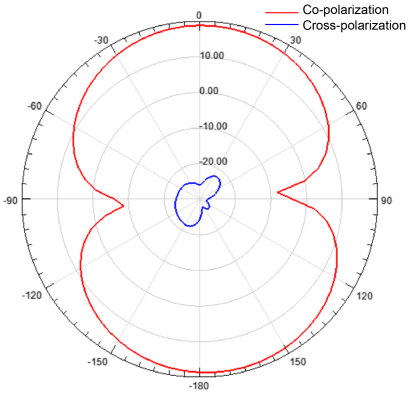

(c) E-plane polar components at 3.286 GHz.

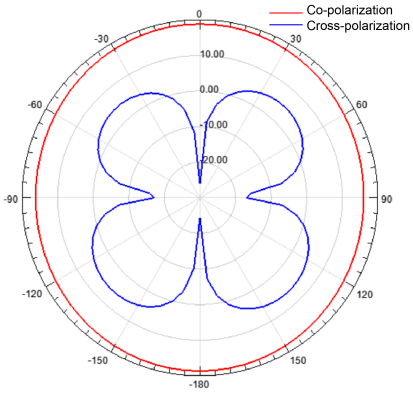

(d) H-plane polar components at 3.286 GHz.

Figure 2.37 Co-polar and cross-polar components of the scaled butterfly antenna at 900 MHz and 3.286 GHz.

Frequency	**Plane**	**Max co-polar component**	**Max cross-polar component**	**HPBW**	**Max Directivity**	**Max Gain**
900 MHz	E($\phi = 90°$)	10.58 dB at $\theta = 0°$	-40.53 dB at $\theta = 105°$	86°	-6.85 dB at $\theta = 0°$	-7.01 dB at $\theta = 0°$
	H($\phi = 0°$)	10.58 dB at $\theta = 0°$	-18.75 dB at $\theta = 130°$	Circle	-6.85 dB at $\theta = 0°$	-7.01 dB at $\theta = 0°$
3.286 GHz	E($\phi = 90°$)	18.83 dB at $\theta = 0°$	-21.79 dB at $\theta = -150°$	82°	1.76 dB at $\theta = 170°$	1.10 dB at $\theta = 170°$
	H($\phi = 0°$)	18.83 dB at $\theta = 0°$	6.22 dB at $\theta = 135°$	Circle	1.73 dB at $\theta = 0°$	1.07 dB at $\theta = 0°$

Table 2.6 Butterfly scaled monopole antenna at 900 MHz and 3.286 GHz.

2.5 Antennas Realization and measurements

In this section, the proposed antennas shown in Figures 2.19 and 2.25 have been fabricated and subjected to experimental testing. Unfortunately, the antennas fabrication process have been done outside the institute using chemical procedures, which make the specific details regarding the exact characteristics of the FR-4 material used in the fabrication unavailable. Therefore, there may be some degree of uncertainty compared to the simulation results. Figure 2.38 depicts the fabricated antennas.

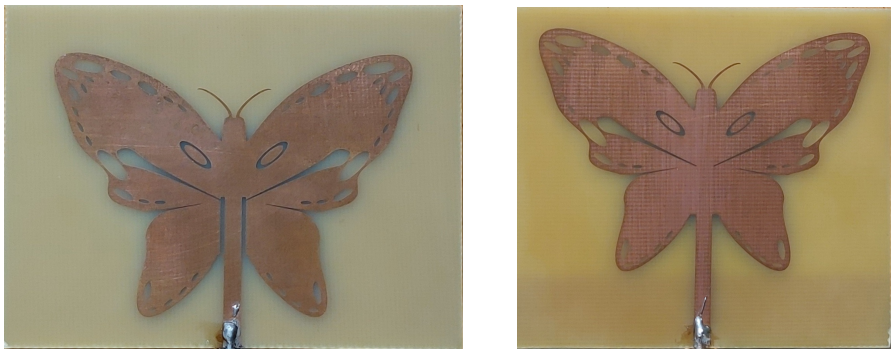

(a) Microstrip butterfly patch antenna. **(b)** Monopole butterfly patch antenna.

Figure 2.38 Fabricated microstrip and monopole butterfly antennas.

The input reflection coefficient of each antenna has been measured using ROHDE & SCHWARZ ZNB20 Vector Network analyzer 100KHz-20GHz provided in the telecommunications laboratory of the institute. Both the simulated and measured $|S_{11}|$ in dB are plotted and shown in Figures 2.39 and 2.40.

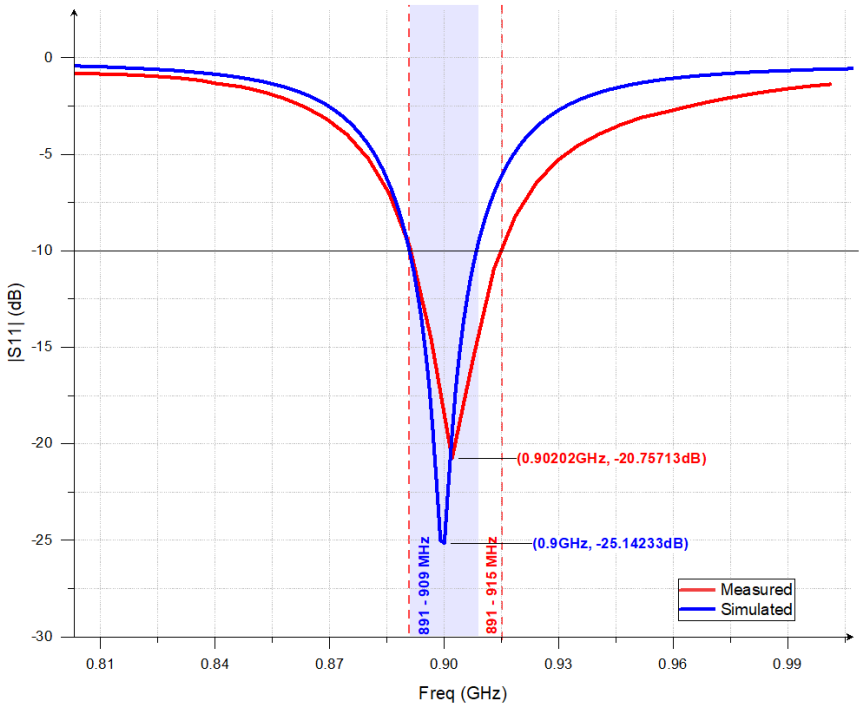

Figure 2.39 Simulated and measured input reflection coefficient of the microstrip butterfly patch.

As can be seen from Figure 2.39, the simulated and the measured results are almost similar with a slight shift of around 0.22% in the resonant frequency. The measured bandwidth is somewhat larger than the simulated one (2.66% measured bandwidth compared to 2% simulated bandwidth). These differences can be attributed to the dielectric material used in the manufacturing of the antenna, which may have a relative permittivity different from the simulation material, the substrate thickness may be different (1.56 mm in the simulation and 1.53 mm in the fabrication), the soldering method and the measuring environment containing the reflecting objects.

Also, the input reflection coefficient of the monopole butterfly antenna is measured and compared with the simulation. The obtained results are shown in Figure 2.40. The figure illustrates some differences between the simulatedand measured results which may be attributed to the same factors stated previously in the microstrip butterfly case. But, the measured reflection coefficient indicates the large band character of the structure with a bandwidth of 116.61%.

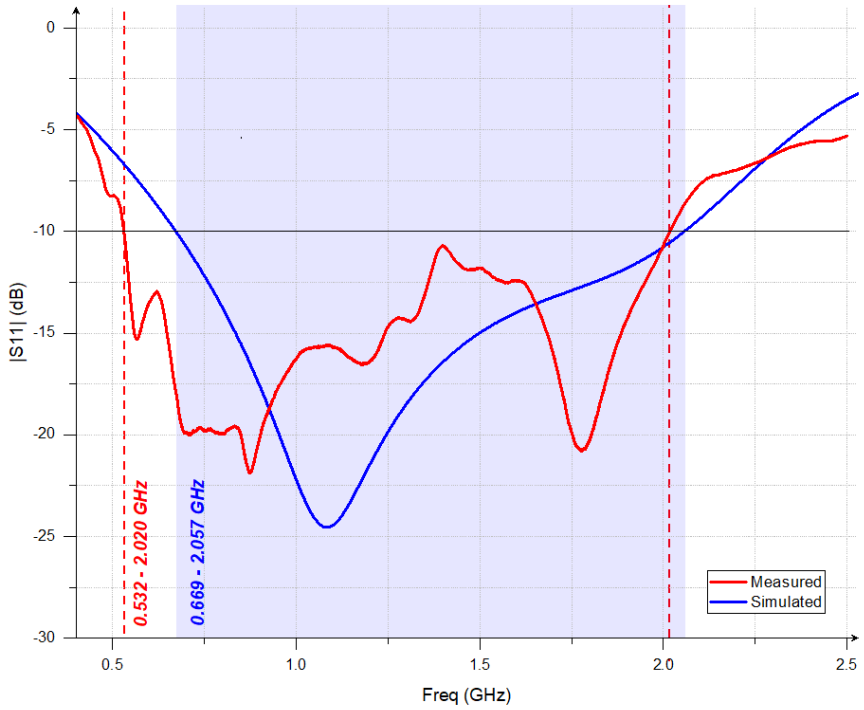

Figure 2.40 Simulated and measured input reflection coefficient of the monopole butterfly patch.

2.6 Conclusion

In conclusion, the improved butterfly form has resulted in a miniaturized structure. This structure has proven its functioning as both a microstrip structure and a monopole. Rigorous measurements have been conducted, validating the usefulness of these realized antennas. These antennas will serve as the fundamental elements in the MIMO systems, which will be further investigated in the subsequent chapter.

Chapter 3

MIMO System

3.1 Introduction

MIMO, or Multiple-Input-Multiple-Output, is widely used in wireless systems. It is a cutting-edge technology that uses multiple transmit and receive antennas to achieve multipath propagation and meet the higher data rate and higher quality demands of modern wireless communications. MIMO systems are a practical technique for sending and receiving multiple independent channels over the same radio channel at the same time using multiple antenna topologies with no extra radiation power loss in a densely scattered environment [12] [13].

3.2 Design of a MIMO System for Space Diversity

In this section, the focus is on designing a 2×1 Multiple-Input Multiple-Output (MIMO) system for space diversity (antennas have the same polarization). Two MIMO systems are designed in this section: one using the microstrip butterfly patch, and the other one using the monopole butterfly patch (see Figures 2.19 and 2.25).

3.2.1 MIMO System Using the Microstrip Butterfly Patch

The MIMO system consists of two parallel placed butterfly patches presented in Figure 3.1a distant by d_{12}, the distance from one feed-line to the other, and a ground covering the two patches as illustrated in Figure 3.1b below. The distance between the two adjacent wings, denoted d', is then found as $d' = d_{12} - 2 \times 31.5$ (mm) as shown in Figure 3.1a.

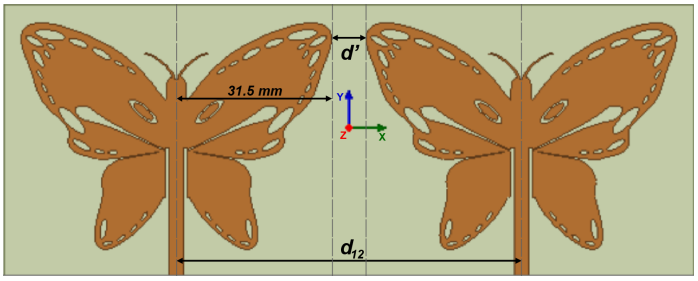

(a) Front view.

(b) Bottom view.

Figure 3.1 2×1 MIMO system with microstrip butterfly patch.

3.2.1.1 Parametric Study on d_{12}

A parametric study is conducted to determine the minimum distance, d_{12}, required to achieve both good matching at 900 MHz and good isolation. The results of this study are shown in Figure 3.2 which illustrates the magnitudes of the input reflection coefficient, S_{11}, and the transmission parameter, S_{12}. It is important to note that the antenna's symmetry and reciprocity properties ensure that S_{11} and S_{22}, as well as S_{12} and S_{21}, are identical.

From the figure, it is evident that even at the closest possible distance, $d' = 0$ mm, the antenna maintains both a high level of matching at 900 MHz (-17.65 dB) and isolation (-43 dB) without isolating the structure. These results suggests a name of a ***self-isolated MIMO antenna***.

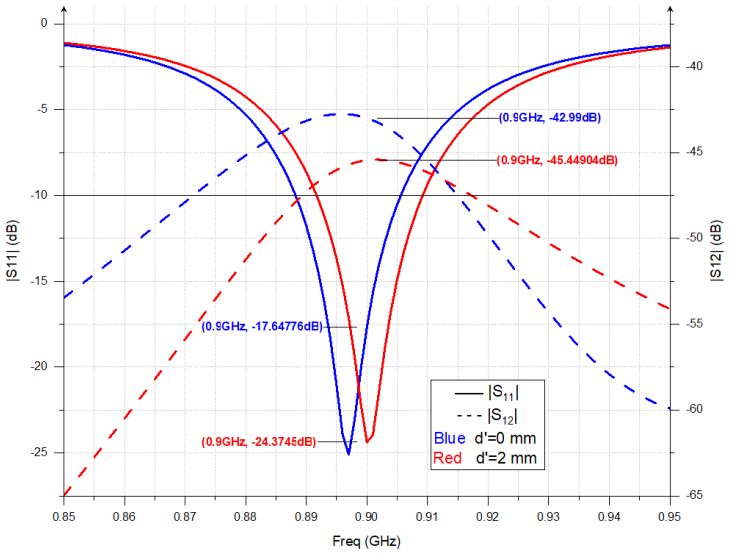

Figure 3.2 *S*-parameters of the MIMO antenna with microstrip butterfly patches for different values of d'.

To account for fabrication tolerances and potential inaccuracies, a distance of $d' = 2$ mm is selected during the fabrication process. The simulated and fabricated MIMO antenna is presented in Figure 3.3. This figure demonstrates the antenna design as it was modeled and then implemented in the physical form. Figure 3.3b represents the fabricated MIMO antenna.

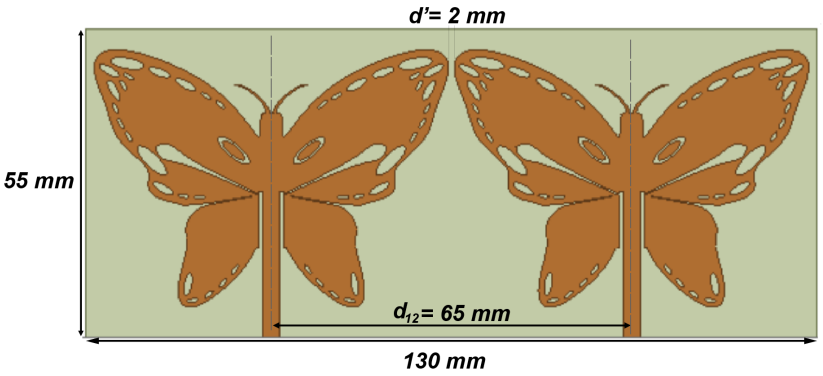

(a) Designed MIMO antenna.

(b) Fabricated MIMO antenna.

Figure 3.3 Proposed 2×1 MIMO antenna with microstrip butterfly patches.

3.2.1.2 Surface Current Distribution

An effective method to observe the interaction between the elements of the MIMO antenna is to analyze the surface current distribution. In Figure 3.4, the distribution of the surface current on the antenna elements is illustrated when only one element is fed. Notably, despite the close proximity of the elements, one of the elements exhibits a complete absence of current along its surface. This observation highlights the self-isolation property of the proposed MIMO antenna.

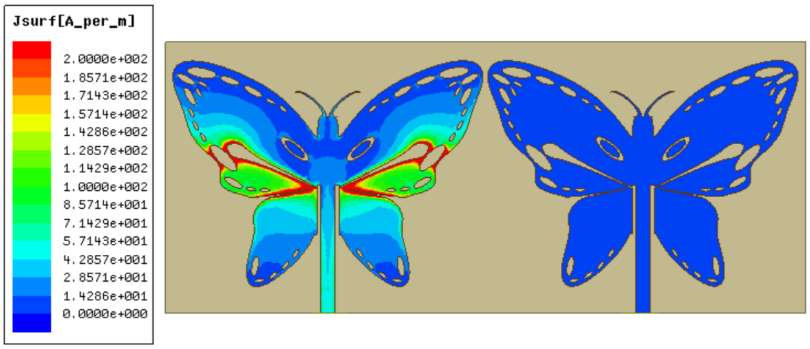

Figure 3.4 Surface current distribution of the proposed MIMO antenna with microstrip butterfly patches.

3.2.1.3 Radiation Patterns

Figure 3.5 illustrates the 3D radiation pattern of an element of the MIMO antenna and it is taken from different views. It is apparent that it is similar to the one of the single proposed antenna with a small deviation in the maximum radiation direction (10° from the broadside). This deviation is due to the presence of the second patch acting as a reflector, and it does not disturb the broadside operation of the structure since the $\theta = 0°$ direction is within the HPBW. These remarks are well illustrated by the 2D cutting shown in Figure 3.6.

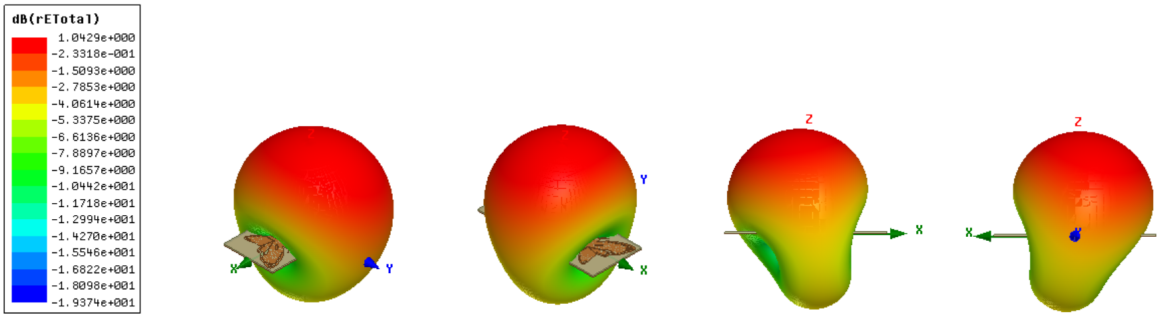

Figure 3.5 3D polar radiation pattern of the proposed MIMO antenna with microstrip butterfly patches.

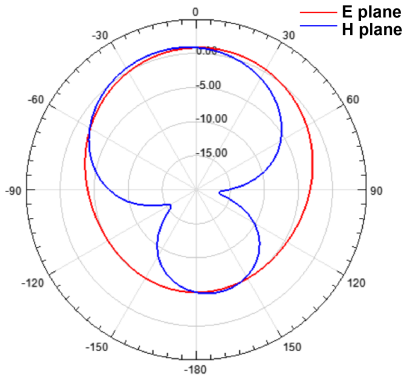

Figure 3.6 E and H field patterns of the proposed MIMO antenna with microstrip butterfly patches in dB.

The co- polar and cross-polar components are presented in Figure 3.7, and the details are summarized in Table 3.1.

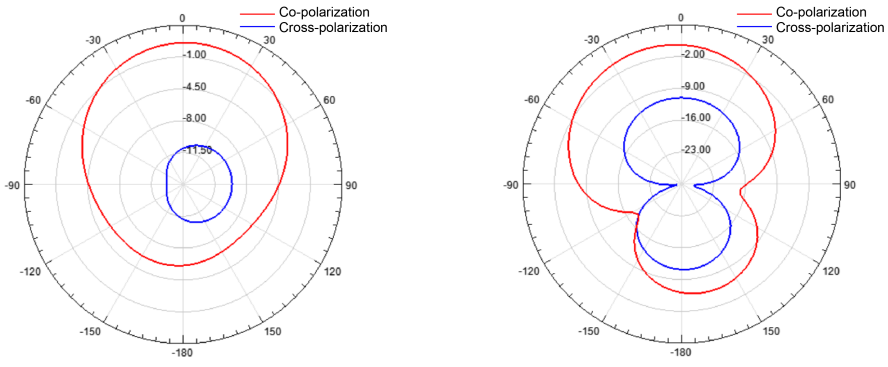

(a) E ($\phi = 90°$). **(b)** H ($\phi = 0°$).

Figure 3.7 Co-polar and cross-polar components of the E and H fields of the proposed MIMO antenna with microstrip butterfly patches in dB.

Plane	Max co-polar component	Max cross-polar component	HPBW	Max Directivity	Max Gain
E($\phi = 90°$)	0.59 dB at $\theta = 5°$	-9.61 dB at $\theta = 85°$	135°	-3.91 dB at $\theta = 10°$	-16.87 dB at $\theta = 10°$
H($\phi = 0°$)	0.75 dB at $\theta = -10°$	-11.04 dB at $\theta = 0°$	98°	-3.77 dB at $\theta = -10°$	-16.73 dB at $\theta = -10°$

Table 3.1 2×1 MIMO Butterfly microstrip antenna at 900 MHz.

3.2.1.4 *S*-Parameters Measurements

Figure 3.8 demonstrates the simulated and measured magnitudes of the *S*-parameters of the fabricated MIMO antenna. Unfortunately, the resonant frequency is shifted by 2.11% from 900 MHz; leading to a non-capability of operating at this frequency. The shift is due to, in addition to the stated factors, the procedure of simulation that should be rectified. The rectification requires the use of SMA connector in the simulation rather than wave port. We noticed this remark lately, and due to the lack of time, we did not proceed to provide new result (re-simulation using SMA connectors). It is advisable to use the SMA connector rather than wave port in simulations. Despite the shift in frequency, the elements of the MIMO antenna works around 881 MHz with satisfactory matching (-14.57 dB) and isolation (-37.5 dB).

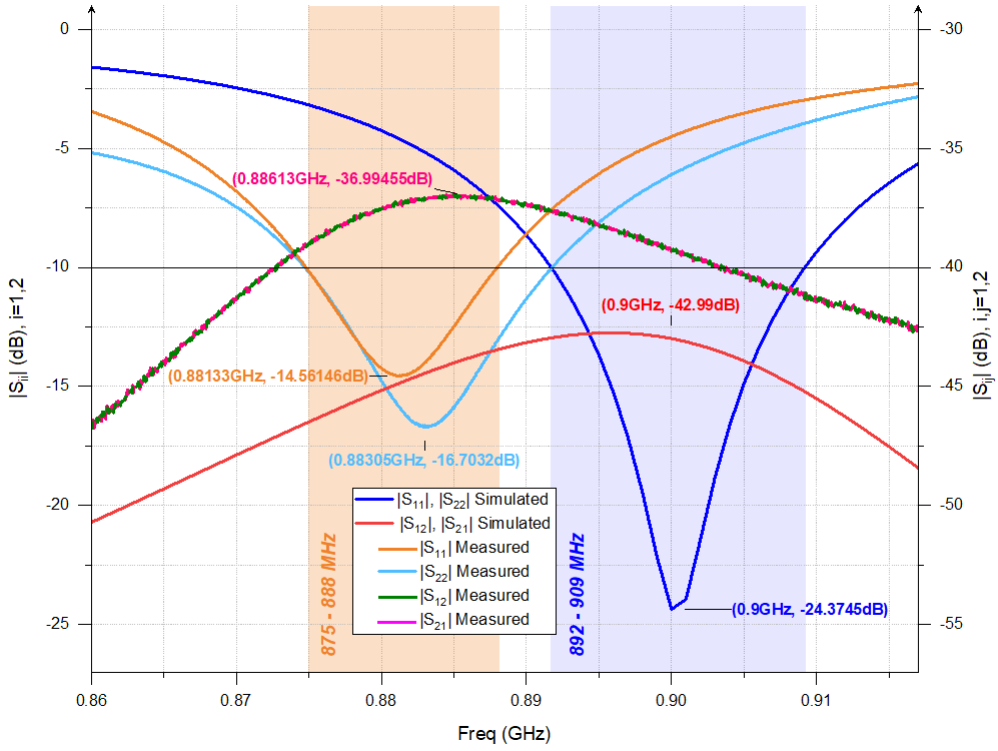

Figure 3.8 Simulated and measured *S*-parameters of the fabricated MIMO microstrip butterfly antenna.

3.2.1.5 MIMO Performance Parameters

To evaluate the effectiveness of the MIMO antenna, the performance measures discussed in Chapter 1 are plotted and analyzed.

Envelope Correlation Coefficient

Figure 3.9 illustrates the simulated and measured Envelope Correlation Coefficient, ECC, of the MIMO antenna. The graph demonstrates the close agreement between the simulated and measured ECC values, validating the accuracy of the simulation. Furthermore, the ECC values indicate that the antenna elements are uncorrelated, as the ECC value is less than 10^{-5} at the simulated and measured resonant frequencies.

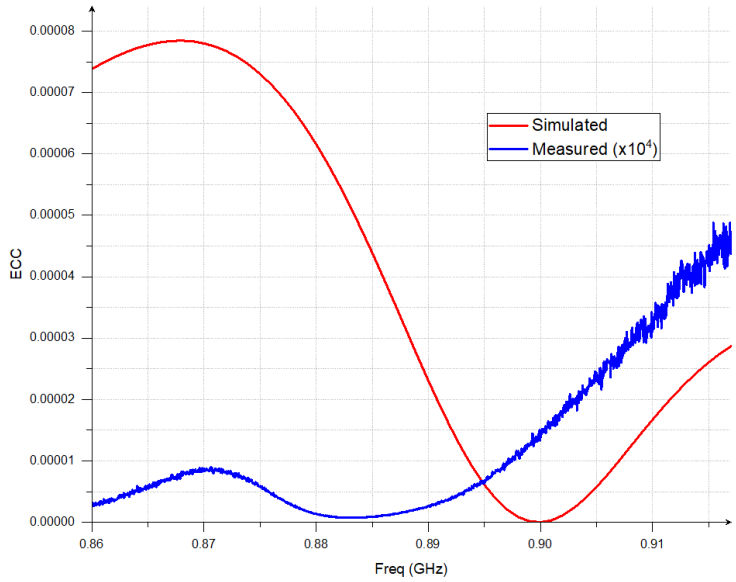

Figure 3.9 Simulated and measured ECC of the fabricated MIMO microstrip butterfly antenna.

Diversity Gain

Since ECC is negligible (almost zero), the Diversity Gain, DG, is 10. This is illustrated in Figure 3.10 where the simulated and measured DG are plotted.

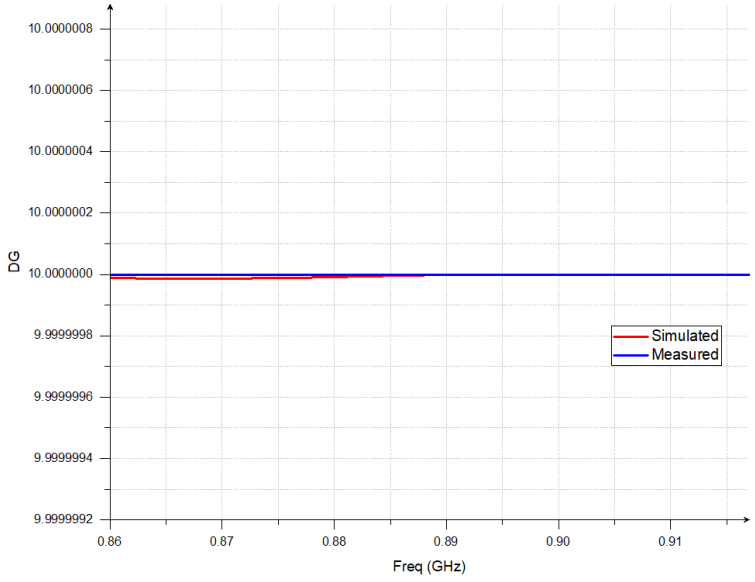

Figure 3.10 Simulated and measured DG of the fabricated MIMO antenna.

Total Active Reflection Coefficient

Figure 3.11 illustrates the simulated and measured Total Active Reflection Coefficient (TARC) of the MIMO antenna when the excitation phase is zero. The TARC exhibits similar behavior to the simulated and measured reflection coefficients S_{11} and S_{22}, as shown in Figure 3.8, and it is less than -10 dB which meets the criteria for MIMO performance. This similarity indicates that the mutual coupling between the MIMO elements is low, which supports the proposition of a self-isolation property of the antenna.

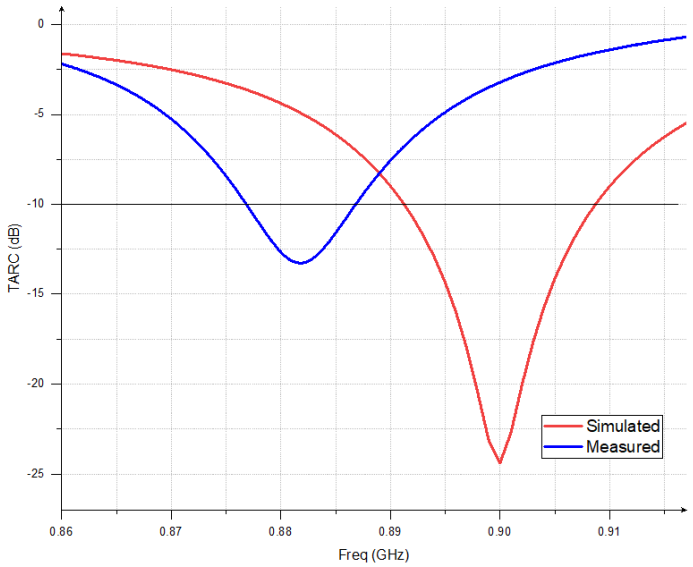

Figure 3.11 Simulated and measured TARC of the fabricated MIMO antenna ($\theta = 0°$).

Channel Capacity Loss

The simulated and measured Channel Capacity Loss, CCL, is depicted in Figure 3.12.

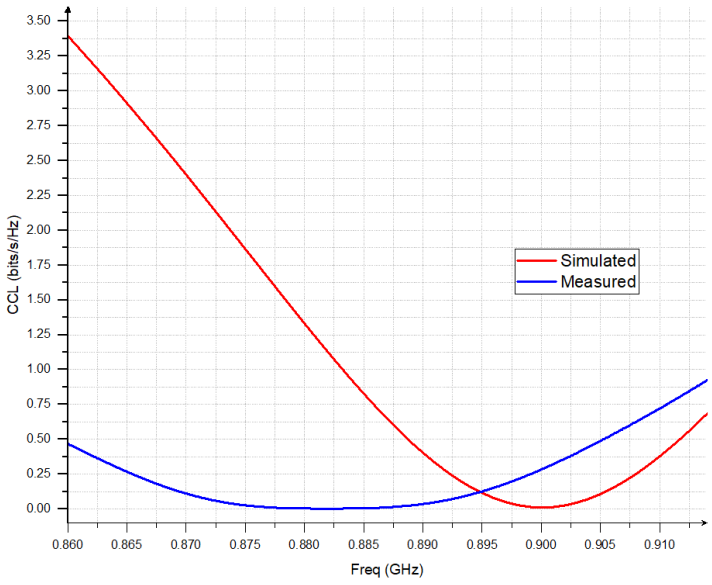

Figure 3.12 Simulated and measured CCL of the fabricated MIMO antenna.

The channel capacity degradation is related to the presence of mutual coupling in a MIMO system. However, in the case of the proposed MIMO antenna, the loss in channel capacity remains below the maximum acceptable value of 0.4 bits/s/Hz. As depicted in Figure 3.12, both the measured and simulated Channel Capacity Loss (CCL) do not exceed 0.02 bits/s/Hz and 0.33 bits/s/Hz, respectively. These results further validate that the antenna is indeed self-isolated.

Mean Effective Gain

Another crucial parameter to consider is the mean effective gain (MEG) of the MIMO antenna. Figure 3.13 displays the simulated and measured MEGs of the MIMO antenna. Notably, it is evident that the MEG consistently reaches the value of -3 dB across the simulated and measured bandwidths. This target MEG value demonstrates the antenna's good performance and indicates its effectiveness in providing a balanced and satisfactory gain throughout the frequency range.

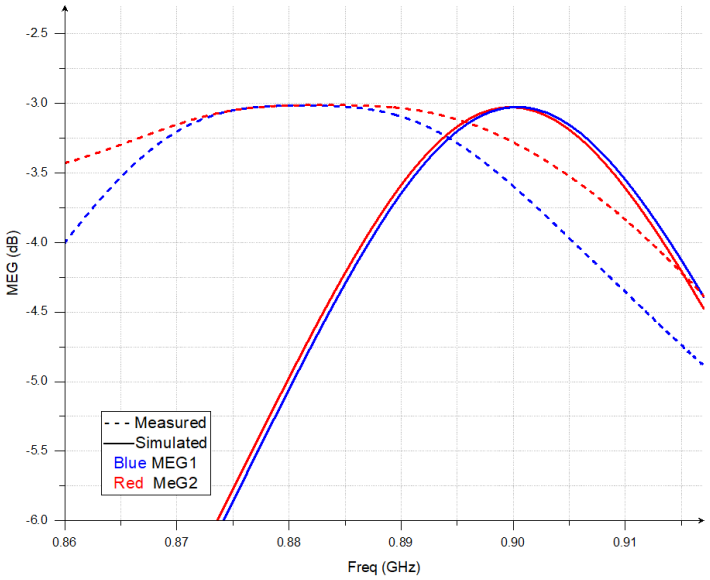

Figure 3.13 Simulated and measured MEGs of the fabricated MIMO antenna.

3.2.2 MIMO System Using the Monopole Butterfly Patch

The positive results obtained from the previously proposed MIMO antenna have acted as a motivator for the design of another MIMO antenna based on the monopole butterfly antenna presented in Chapter 2.

The design of the 2×1 MIMO antenna consists of two monopole butterfly antennas (Figure 2.25) positioned in parallel and in close proximity to each other as depicted in Figure 3.14. To investigate the impact of antenna spacing on the performance of the MIMO system, a parametric study on the distance between the antennas is conducted.

Similar to the previous section, the study establishes a relationship between the distance between the adjacent upper wings, denoted as d', and the distance between the feed lines, denoted as d_{12}. Specifically, the relation is given as $d' = d_{12} - 2 \times 31.5$ (mm).

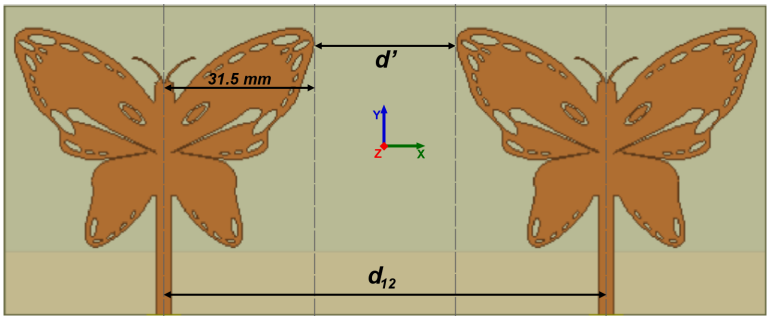

(a) Front view.

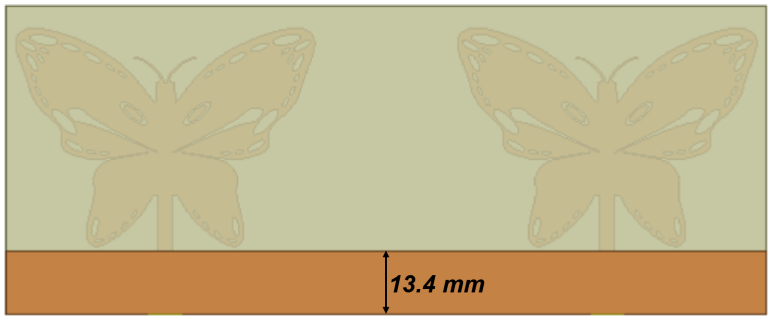

(b) Bottom view.

Figure 3.14 The 2×1 MIMO system as designed for space diversity.

3.2.2.1 Parametric Study on d_{12}

By conducting a parametric study on the distance d_{12} and examining the simulated S-parameters, it has been observed that the MIMO antenna being discussed in this section differs from the previous one. Unlike the previous MIMO antenna design, it is not applicable to have a zero distance between the adjacent upper wings ($d' = 0$ mm) in this case.

Figure 3.15 illustrates the simulated S-parameters of the MIMO antenna for different values of the distance d'.

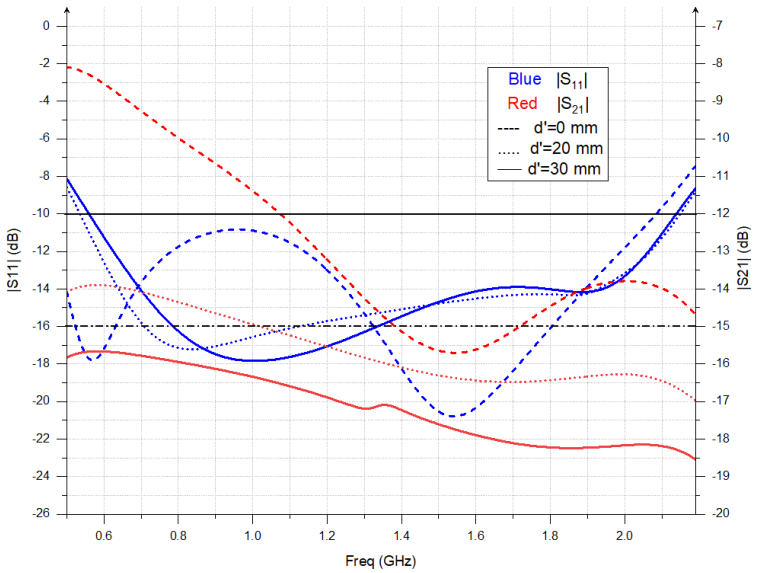

Figure 3.15 S-parameters of the MIMO antenna with monopoles for different values of d'.

The observations from the simulated S-parameters reveal that for $d' = 0$ mm, the transmission coefficient exceeds -15 dB, indicating the presence of significant mutual coupling between the antennas. Hence, it is important to consider an appropriate distance d_{12} that ensures sufficient isolation between the antennas in order to minimize mutual coupling effects and optimize the performance of the MIMO antenna system.

Based on the analysis presented in Figure 3.15, it can be concluded that a value of $d' = 30$ mm$= 0.148\lambda$ (λ at 900 MHz) seems to be an appropriate choice for maintaining a compact antenna size while ensuring that the level of mutual coupling remains below -15 dB. This threshold is typically considered as the minimum requirement for achieving effective isolation between the antenna elements. Figure 3.16 depicts the final structure of the fabricated MIMO antenna.

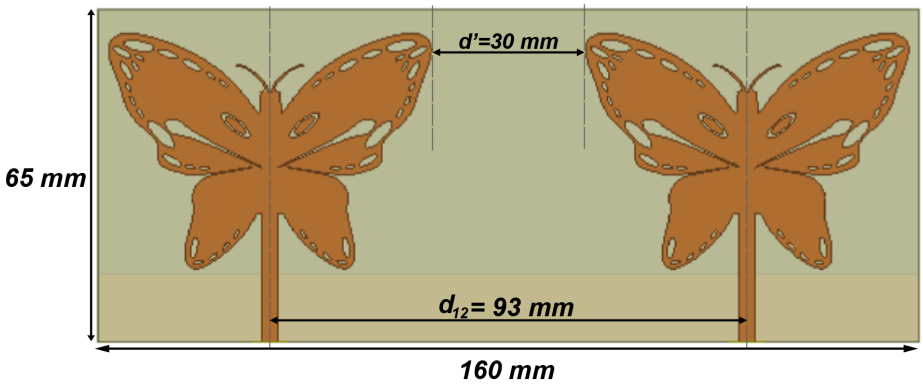

(a) Designed MIMO antenna.

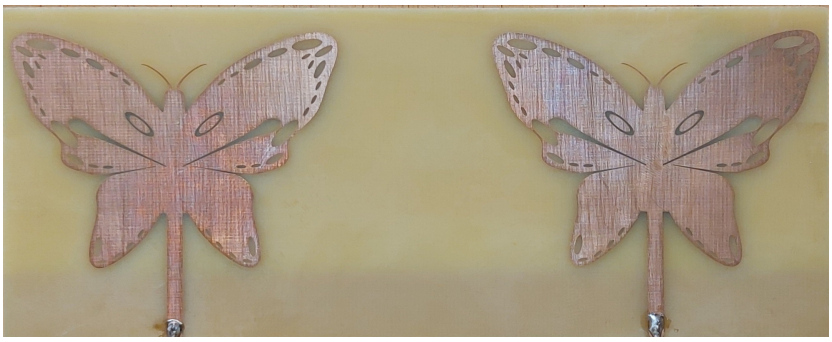

(b) Fabricated MIMO antenna.

Figure 3.16 2×1 MIMO system as designed for space diversity using monopole butterfly patches.

3.2.2.2 Surface Current Distribution

An interesting observation can be made when examining the surface current distribution of the MIMO antenna in Figure 3.16. Unlike the microstrip case, the figure shows that some induced current on the second patch exists even though the separation distance is increased. This is due to the absence of the ground and the high cross polarized components in the excited patch. This suggests, for future work, the addition of properly designed isolators.

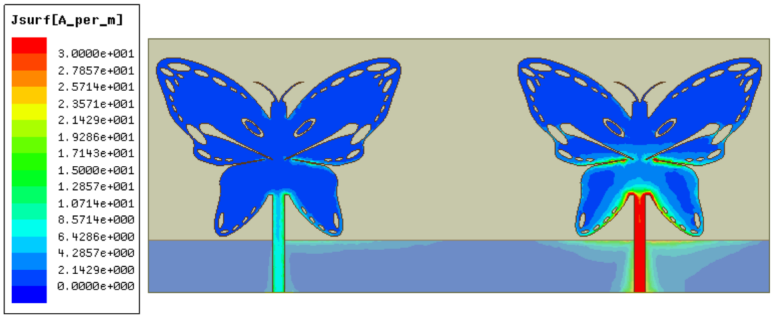

Figure 3.17 Surface current distribution of the MIMO antenna with monopole butterfly patches.

3.2.2.3 Radiation Patterns

The radiation patterns illustrated in Figures 3.18 and 3.19. show almost the same radiation properties as compared to the monopole butterfly antenna. The difference is in the maximum radiation direction that is shifted due to the presence of the second patch in the neighborhood of the first patch, in addition to the higher levels of the cross polar components as presented in Figure 3.20.

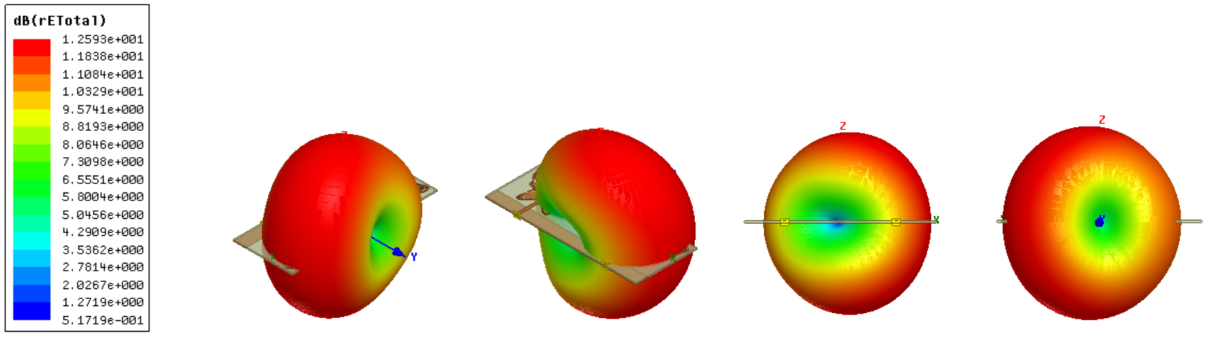

Figure 3.18 3D radiation pattern of the MIMO antenna with monopole butterfly patches.

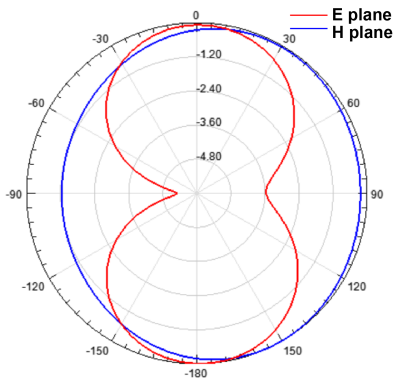

Figure 3.19 E and H field patterns of the MIMO antenna.

Figure 3.20 illustrates the co-polar and cross-polar components of the MIMO dipoles. The specific details and findings are summarized in Table 3.2.

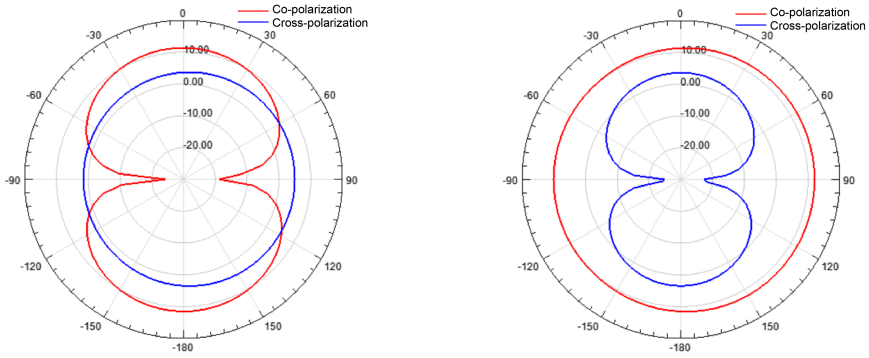

(a) E ($\phi = 90°$). **(b)** H ($\phi = 0°$).

Figure 3.20 Co-polar and cross-polar components of the E and H fields in dB.

Plane	Max co-polar component	Max cross-polar component	HPBW	Max Directivity	Max Gain
E($\phi = 90°$)	11.52 dB at $\theta = 180°$	5.02 dB at $\theta = 85°$	92°	-5.29 dB at $\theta = 175°$	-5.41 dB at $\theta = 175°$
H($\phi = 0°$)	12.22 dB at $\theta = 135°$	3.64 dB at $\theta = 0°$	Circle	-4.93dB at $\theta = 150°$	-5.05 dB at $\theta = 150°$

Table 3.2 2×1 MIMO Butterfly microstrip antenna at 900 MHz.

3.2.2.4 *S*-Parameters Measurements

To validate the obtained simulated results, the *S*-parameters of the MIMO antenna are measured and the results are shown in Figure 3.21.

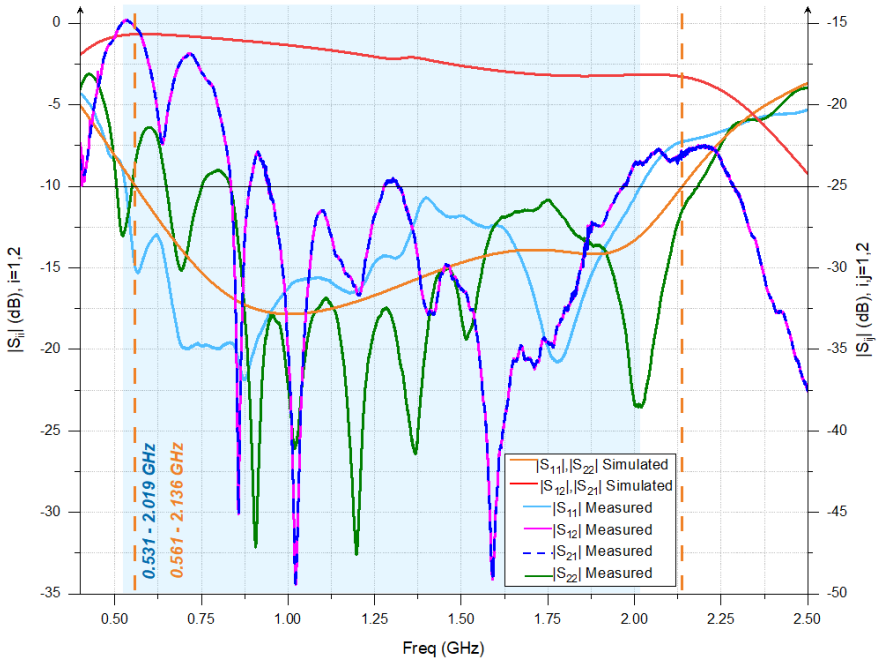

Figure 3.21 Simulated and measured *S*-parameters of the MIMO antenna with monopole butterfly patches.

In the comparison, some shift can be observed in the lower and higher frequencies of the measured

operating bandwidth as compared to the simulated results. In addition, there is some disparity in the input reflection coefficients of the patches. Furthermore, although the coupling is lower than −15 dB, it affects the operation of the structure. Again, an isolator is suggested.

In addition to mutual coupling, there are several other factors that can contribute to the deviations. These factors include the dielectric material used in the fabrication, which may have a different permittivity compared to the one used in the simulation and its thickness. Additionally, factors such as uncertainties in the realization process (as slots may not be exact, requiring the use of a laser PCB machine), soldering effects, and the measurement environment can also have an effect on the results.

3.2.2.5 MIMO Performance Parameters

Similar to the approach followed in the previous section of this chapter, the MIMO antenna effectiveness is evaluated through the parameters discussed in Chapter 1.

Envelope Correlation Coefficient

In Figure 3.22, both the simulated and measured ECC of the MIMO antenna are depicted. It is worth noting that the ECC values for this MIMO antenna are higher compared to the MIMO antenna proposed in the previous section. However, despite the increase, the ECC results are still significantly smaller than the nominal value of 0.5 indicating an acceptable coupling between the antenna elements.

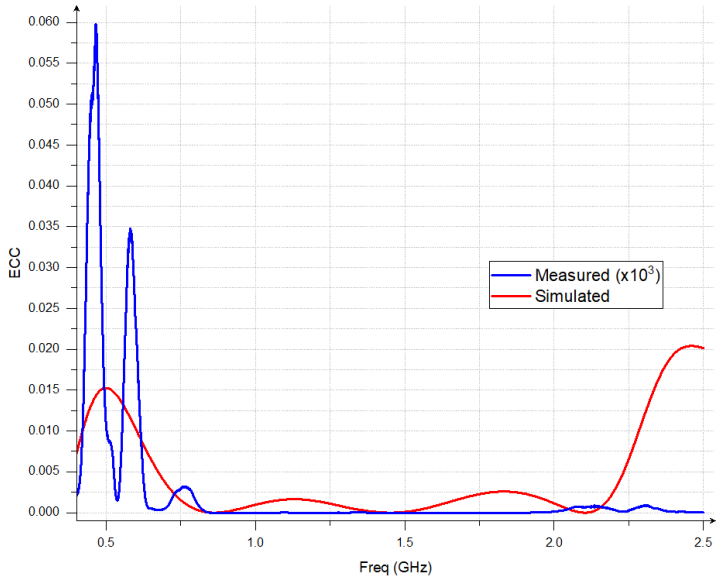

Figure 3.22 Simulated and measured ECC of the MIMO antenna with monopole butterfly patches.

Diversity Gain

Based on the ECC presented above, the Diversity Gain is calculated, plotted, and demonstrated in Figure 3.23. These results indicate the acceptable level of isolation since the DG is almost 10.

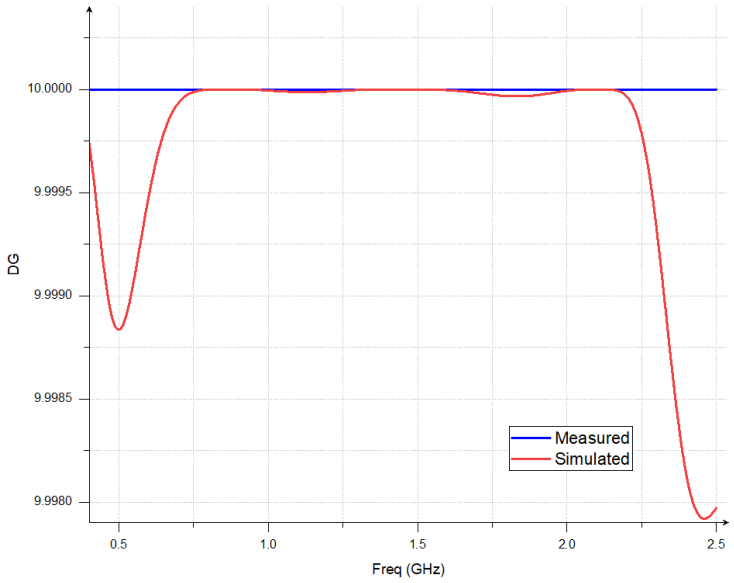

Figure 3.23 Simulated and measured DG of the MIMO antenna with monopole butterfly patches.

Total Active Reflection Coefficient

Figure 3.24 displays the TARC graphs of the MIMO antenna. The observed behavior of the TARC graphs closely resembles that of the input reflection coefficients shown earlier, thereby confirming an acceptable level of mutual coupling.

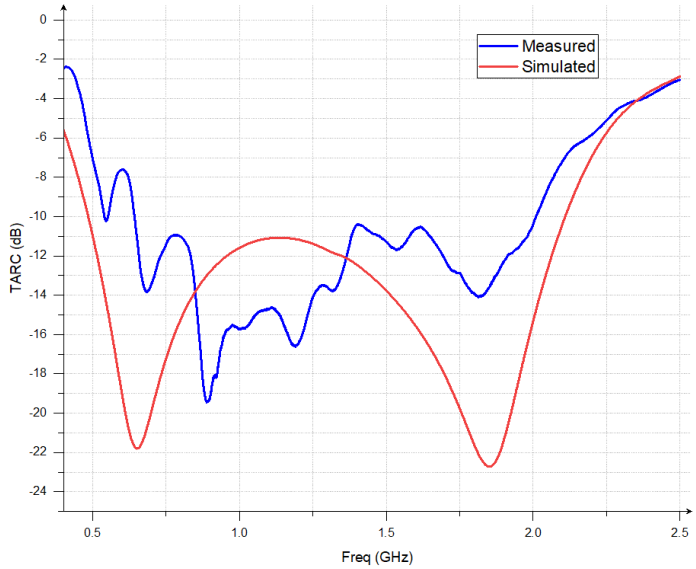

Figure 3.24 Simulated and measured TARC of the MIMO antenna with monopole butterfly patches.

Channel Capacity Loss

The reduction in channel capacity is due to various factors, including mutual coupling. Figure 3.25 depicts the simulated and measured CCL of the MIMO antenna. It is evident from the graph that the observed loss does not exceed the specified threshold of 0.4 bit/s/Hz throught both

the simulated and measured bandwidths. This indicates that the MIMO antenna exhibits a low channel capacity loss.

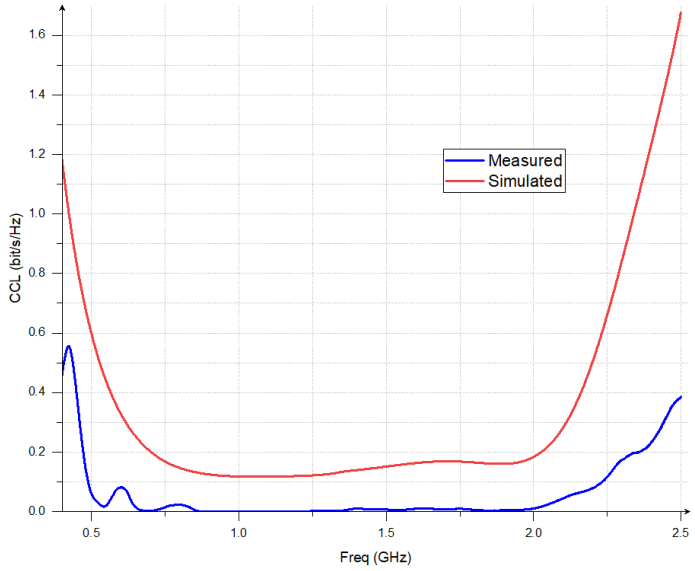

Figure 3.25 Simulated and measured CCL of the MIMO antenna with monopole butterfly patches.

Mean Effective Gain

Figure 3.26 provides a visual representation of the MEG across the operating bandwidth of the MIMO antenna. the MEG level is approximately -3 dB, which suggests that the MIMO antenna is performing well across the simulated and measured operating bandwidths.

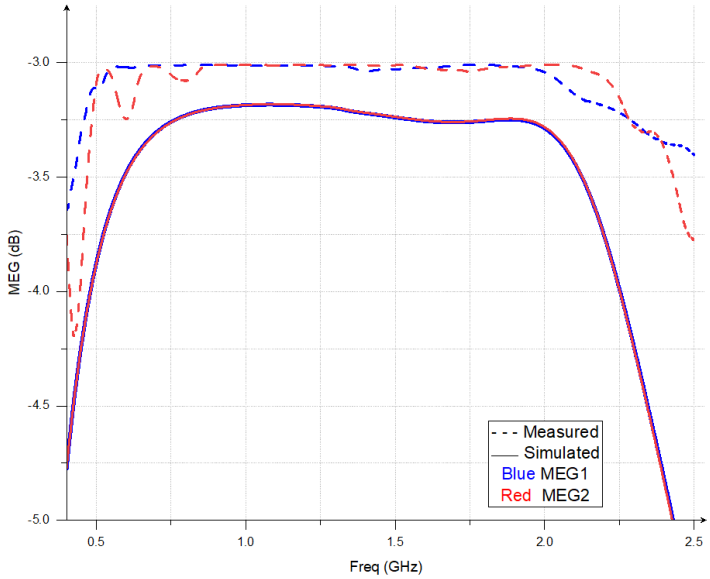

Figure 3.26 Simulated and measured MEG of the MIMO antenna with monopole butterfly patches.

3.3 Comparative Study

For a purpose of situating our contribution to the design of the MIMO antennas using the improved butterfly structure, and due to the absence of the references working at 900 MHz, a rectangular MIMO antenna is designed and simulated. The choice of the rectangular patch is done since it is widely used in practice. The rectangular patch resonates at 900 MHz. The MIMO parameters used in the butterfly case (distance between the elements) are reproduced in the rectangular one. The simulation results are given in Appendices A and B and the results are presented in Table 3.3.

MIMO using	**Size** (mm^2)	**BW (MHz)**	**Matching at 900 MHz**	**Isolation at 900 MHz**	**Max Isolation**	**Max Directivity**	**Max Gain**
Microstrip butterfly	130×55	892 - 909	-24.37dB	-45.45dB	-45.45dB	-3.91dB $\phi = 90°$ $\theta = 5°$	-16.87 dB $\phi = 90°$ $\theta = 5°$
Microstrip rectangular	200×100	895 - 918	-15.06dB	-12.99dB	-12.99dB	1.78dB $\phi = 0°, 90°$ $\theta = 0°$	-3 dB $\phi = 0°, 90°$ $\theta = 0°$
Monopole butterfly	160×65	561 - 2136	-16.12dB	-16.22dB	-15.96dB	-5.29 dB $\phi = 90°$ $\theta = 175°$ -5.41 dB $\phi = 90°$ $\theta = 175°$	-4.93 dB $\phi = 0°$ $\theta = 150°$ -5.05 dB $\phi = 0°$ $\theta = 150°$
Monopole rectangular	228×100	289 - 1215	-14.94dB	-18.01dB	-14.29dB	-4.11 dB $\phi = 90°$ $\theta = 170°$ -4.25 dB $\phi = 90°$ $\theta = 170°$	-3.59 dB $\phi = 0°$ $\theta = 150°$ -3.74 dB $\phi = 0°$ $\theta = 150°$

Table 3.3 Performance comparison of the proposed MIMO Butterfly antennas.

3.4 Conclusion

Two MIMO antenna strcuctures are designed. One uses two microstrip butterfly patches resulting in a self-isolated structure, i.e., no need for isolators. This result is obtained although the physical separation is far lower than half-wavelength required for diversity. The second MIMO antenna uses monopole butterfly patch. While the coupling between the elements is already sufficiently low, the results indicate that incorporating suitable isolators could further enhance the overall performance of the antenna system.

General Conclusion

In this project, improvements in the shape of a butterfly antenna have been proposed. Initially, the design started from a basic microstrip butterfly structure generated using a mathematical formula operating at 1.66 GHz to a modified structure operating at 900 MHz, which results in about 54% size reduction in both the length and the width of the patch. The new structure is obtained by adding several DMS slots to the structure using the super-shape formula and rotated ellipses. The resultant structure is operated as microstrip and monopole antennas. The obtained results demonstrate the ability of the proposed butterfly antennas to radiate energy. However, it is observed that these structures exhibit relatively low gain, which can be attributed to their small size and the presence of multiple slots. To overcome this limitation, the proposed antennas can be utilized in conjunction with an amplifier (active antenna) or integrated into an array system. Furthermore, 2×1 MIMO antenna systems have been designed for space diversity using the microstrip and the monopole butterfly patches. The MIMO-based microstrip antenna has a good reflection coefficient and good isolation without the need to an isolator; resulting in a self-isolated structure. On the other hand, the results of the MIMO monopole butterfly antenna suggests the necessity of isolators.

Since no existing references were found regarding MIMO antennas operating around 900 MHz, a rectangular MIMO design is created for comparison purposes. The proposed design exhibits smaller dimensions and higher isolation compared to its rectangular counterpart.

It is observed that the simulation method employed in the HFSS software influences the accuracy of the measured results. It is recommended to use SMA connectors in the simulation instead of wave ports for improved accuracy.

As part of future work, the following areas of improvement can be explored:

- Enhancing the gain of the antennas (active antennas are suggested).
- Designing the patches with other dielectric materials.
- Exploring the potential of the proposed antennas for other diversities, such as polarization and radiation pattern diversity.
- Extending the proposed structures for array applications, including phased array systems.

Appendices

Appendix A

MIMO Microstrip Rectangular Antenna

The rectangular antenna is designed using an empirical formula [23] to resonate at 900 MHz using FR-4 substrate.The obtained dimensions and the results are summarized in the following figures.

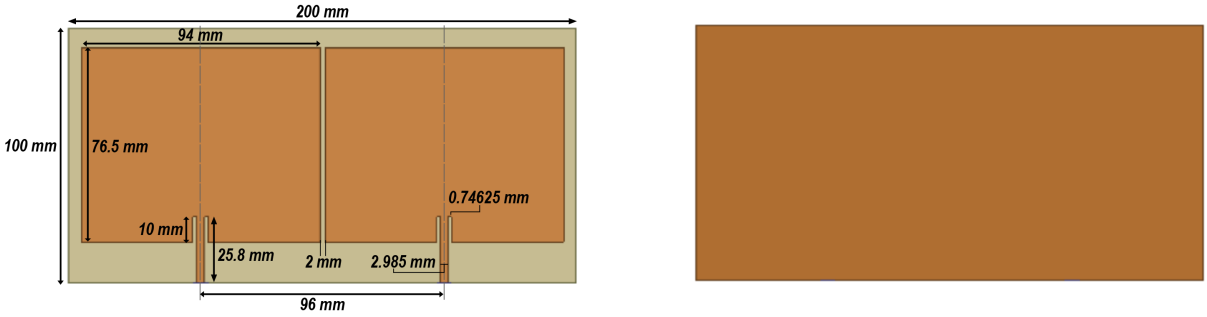

(a) Front view. **(b)** Back view.

Figure A.1 Design of the 2×1 MIMO antenna with microstrip rectangular patches.

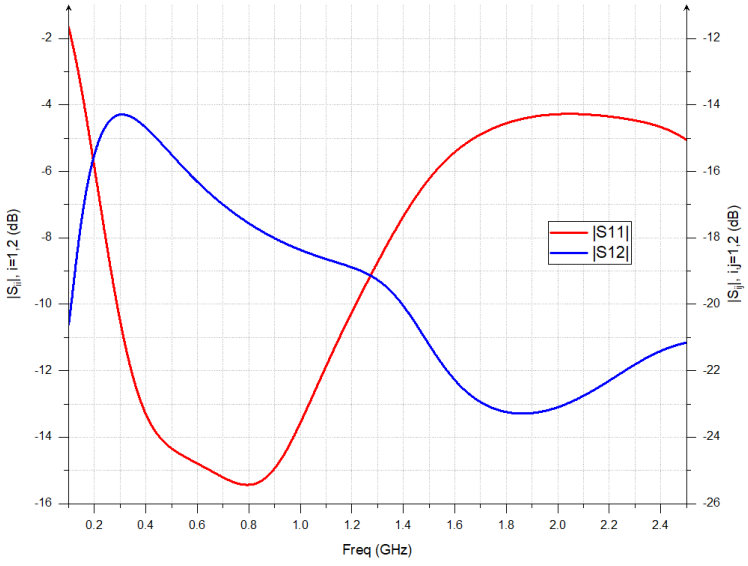

Figure A.2 Simulated S-parameters of the MIMO antenna with microstrip rectangular patches.

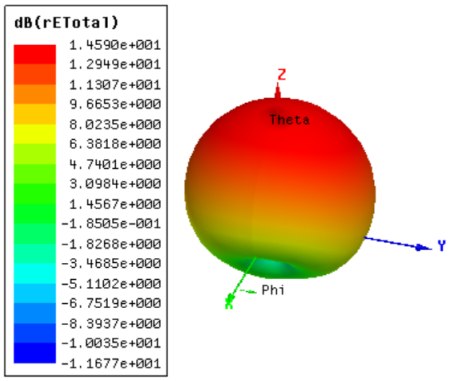

Figure A.3 3D polar radiation pattern of the 2×1 MIMO antenna with microstrip rectangular patches.

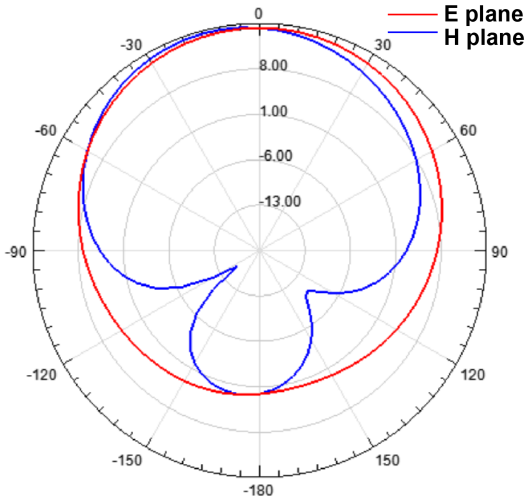

Figure A.4 E and H plane patterns of the 2×1 MIMO antenna with microstrip rectangular patches.

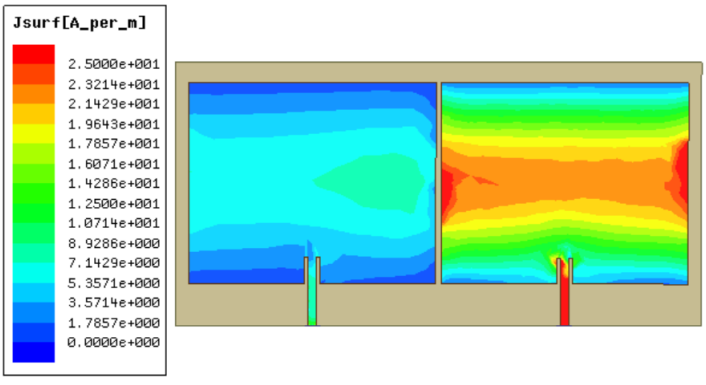

Figure A.5 Surface current distribution of the 2×1 MIMO antenna with microstrip rectangular patches.

Appendix B

MIMO Monopole Rectangular Antenna

The same dimensions of the rectangular patch are kept in this design. The feeding technique is changed to microstrip feed-line, and the ground length is equal to the one used in the MIMO monopole butterfly antenna. The results are illustrated by the following figures.

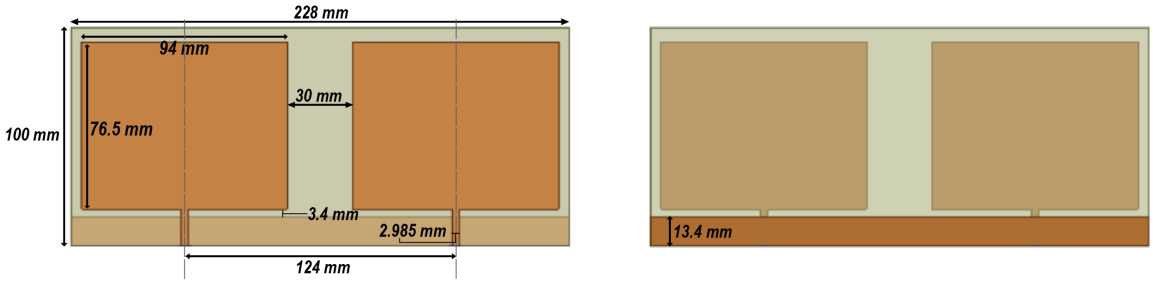

(a) Front view. **(b)** Back view.

Figure B.1 Design of the 2×1 MIMO antenna with monopole rectangular patches.

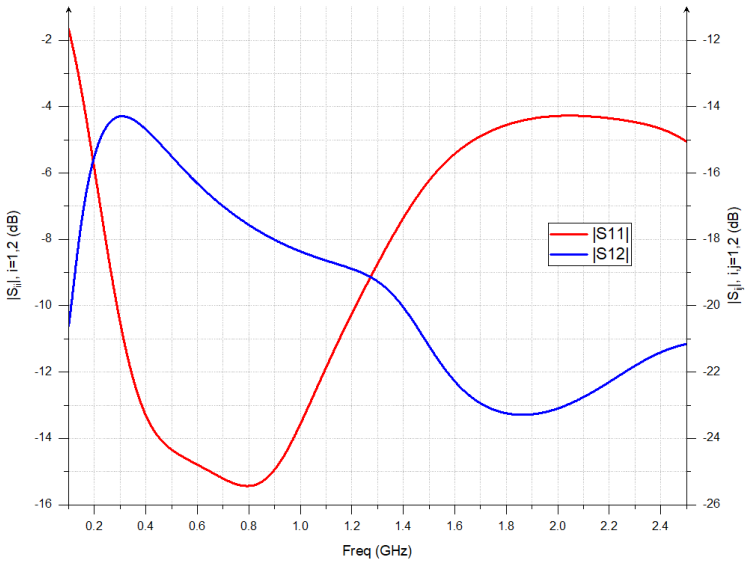

Figure B.2 Simulated S-parameters of the MIMO antenna with monopole rectangular patches.

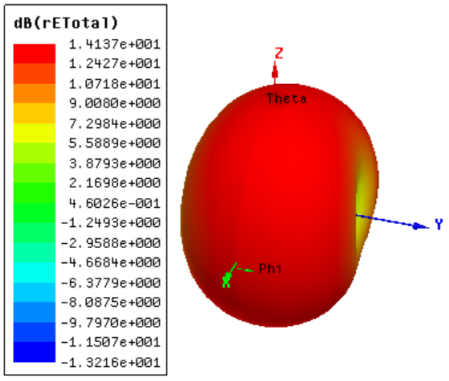

Figure B.3 3D polar radiation pattern of the 2×1 MIMO antenna with monopole rectangular patches.

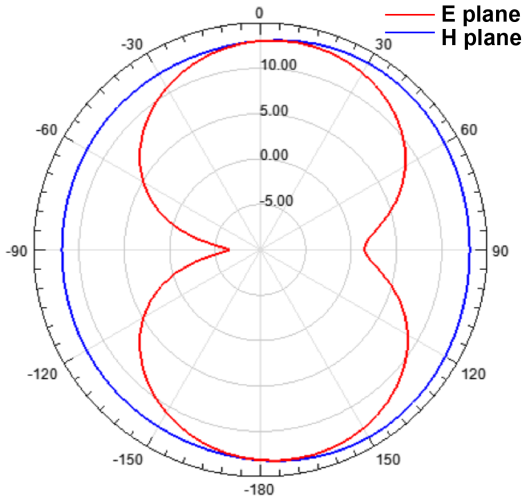

Figure B.4 E and H plane patterns of the 2×1 MIMO antenna with monopole rectangular patches.

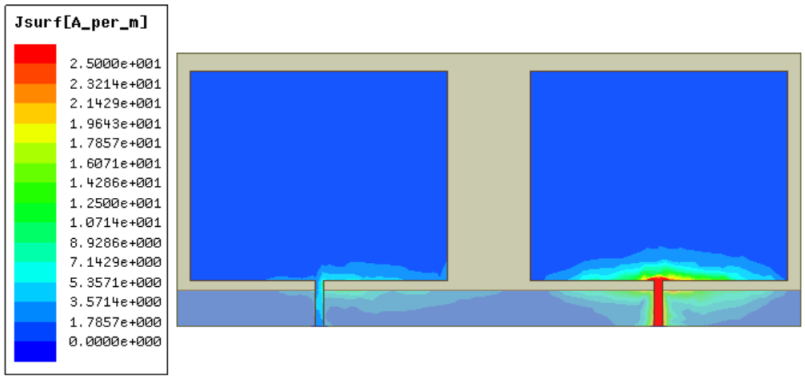

Figure B.5 Surface current distribution of the 2×1 MIMO antenna with monopole rectangular patches.

References

[1] C. A. Balanis, *Antenna Theory: Analysis and Design*, John Willy & Sons, 2016.

[2] A. AZRAR, "Antenna Parameters," Institute of Electrical and Electronic Engineering, University M'Hamed BOUGARA, Boumerdes, 2022.

[3] M. DEHMAS, "Contribution to analysis small microstrip antennas," Ph.D. dissertation, Institute of Electrical and Electronic Engineering, University M'Hamed BOUGARA, 2020.

[4] A. Siblini, "Optimization of Antenna ARMA (Agile Matrix Antenna Radiating by Pixel Elaborated With Meta-material) For Beam Forming for the RFID and Radar Applications," Ph.D. dissertation, 2017.

[5] Ludwig and Arthur, "The Definition of Cross Polarization," *IEEE Transactions on Antennas and Propagation,* vol. 21, no. 1, pp. 116 - 119, 1973.

[6] A. Mehta, "Microstrip Antenna," *International Journal of Scientific & Technology Research,* vol. 4, no. 3, March 2015.

[7] M. Chowdhury, Q. D. Hossain, M. A. Hossain and a. R. C. Cheung, "Single Feed Circularly Polarized Crescent-Cut and Extended Corner Square Microstrip Antennas for Wireless Biotelemetry," *International Journal of Electrical and Computer Engineering,* vol. 9, June 2019.

[8] P. K. Malik, S. Padmanaban and J. B. Holm-Nielsen, *Microstrip Antenna Design for Wireless Applications*, Taylor & Francis Group, 2022.

[9] C. TAOUINT, "Contribution to The Design and Analysis of Butterfly Printed Antenna," M.S. thesis, Institute of Electrical and Electronic Engineering, University M'Hamed BOUGARA Boumerdes , 2022.

[10] M. CHAVALI and M. Nikolova, "Metal Oxide Nanoparticles and Their Applications in Nanotechnology," *SN Applied Sciences,* vol. 1, June 2019.

[11] S. MOUHOUCHE, A. AZRAR, M. DEHMAS and K. DJAFRI, "A Compact Superformula Based Ultra-Wide Band Antenna Shape With Two Notched Bands," *Microwave and Optical Technology Letters,* vol. 60, no. 11, pp. 2693 - 2697, 2018.

[12] A. PAULRAJ, D. GORE, R. NABAR and H. BOLCSKEI, "An Overview of MIMO Communications - a Key to Gigabit Wireless," *Proceedings of the IEEE,* vol. 92, no. 2, pp. 198 - 218, 2004.

[13] I. Nadeem and D. Y. Cho, "Study on Mutual Coupling Reduction Technique for MIMO Antennas," *Proceedings of the IEEE,* December 2018.

[14] "R-Spectrum RadioFrequency Technology," 2022. [Online]. Available: https : / / r - spectrum . com . au / resources / wireless - transmission/mimo/4x4-mimo. [Accessed 01 12 2023].

[15] H. J. Visser, "Antenna Theory and Applications," *John Wiley & Sons,* 2012.

[16] Y. Huang and K. Boyle, "Antennas from Theory to Practice," *John Wiley & Sons,* Chichester, UK, 2008.

[17] Y. Liu, Z. Yang, P. Chen, J. Xiao and Q. Ye, "Solation Enhancement of a Two-Monopole MIMO Antenna Array with Various Parasitic Elements for Sub-6 GHz Applications," *Micromachines,* vol. 13, no. 12, 2022.

[18] M. S. Sharawi, "Printed Multi-Band MIMO Antenna Systems and Their Performance Metrics [wireless corner]," *IEEE Antennas and Propagation Magazine,* vol. 55, no. 5, pp. 218 - 232.

[19] S. Kolangiammal, L. Balaji and M. Mahdal, "A Compact Planar Monopole UWB MIMO Antenna for Short-Range Indoor Applications," *Sensors,* vol. 23, no. 9, p. 4225, April 2023.

[20] B. R. Rao, K. S. Chakradhar and D. Nataraj, "Design, Optimization and Experimental Verification of UWB-MIMO Antenna With WLAN and Complete X-Band Notched Characteristics Checked With Characteristic Mode Analysis (CMA)," *Analog Integrated Circuits and Signa Processing,* vol. 115, no. 1, pp. 139 - 158, February 2023.

[21] A. Pandey, *Practical Microstrip and Printed Antenna Design*, Artech House, 2019.

[22] "JEM Engineering," September 2020. [Online]. Available: https://jemengineering.com/blog-microstrip-antennas-the-basics/. [Accessed 1 15 2023].

[23] M. Z. Rahman, M. Mynuddin and K. C. Debnath, "The Significance of Notch Width on The Performance Parameters of Inset Feed Rectangular Microstrip Patch Antenna," *International Journal of Electromagnetics and Applications,* vol. 10, no. 1, pp. 7 - 18, 2020.

[24] "Observation,"[Online]. Available: https://observation.org/observation/48475124/. [Accessed 1 12 2023].

[25] "Nature,"[Online].Available:https://www.nature.org/en-us/get-involved/how-to-help/animals-we-protect/monarch-butterfly/. [Accessed 01 12 2023].

[26] "Large Skipper (Ochlodes Sylvanus)," [Online]. Available: https://www.britishbutterflyaberrations.co.uk/species/ochlodes-sylvanus/aberrations. [Accessed 01 12 2023].

[27] "FCC," September 2022. [Online]. Available: https://transition.fcc.gov/oet/spectrum/table/fcctable.pdf. [Accessed 01 20 2023].

[28] A. A. Omar, S. Naser, M. I. Hussein, N. I. Dib and M. W. Rashad, "Superformula-Based Compact UWB CPW-Fed-Patch Antenna With and Without Dual Frequency Notches," *ACES JOURNAL,* vol. 32, no. 11, pp. 979 - 986, 2017.

[29] E. Okon, B. Allen, W. Malik, M. Dohler, A. Brown and D. Edwards, *Ultra Wideband Antennas and Propagation for Communications, Radar and Imaging*, John Wiley & Sons, 2006.